YTUP

Journal of Thermal Engineering
https://jten.yildiz.edu.tr/
https://doi.org/10.47481/jten.0082

RESEARCH ARTICLE

Impact of refractory elements design on heat transfer in the combustion chamber of wood-log gasification boilers

Rade M. Karamarković[1], Đorđe A. Novčić[2], Miloš V. Nikolić[3,*], Dušan M. Todorović[4], Marko O. Obradović[5]

[1]Faculty of Mechanical and Civil Engineering in Kraljevo, University of Kragujevac, Dositejeva 19, 36000, Kraljevo, Serbia
[2]Faculty of Mechanical and Civil Engineering in Kraljevo, University of Kragujevac, Dositejeva 19, 36000, Kraljevo, Serbia
[3]Faculty of Mechanical and Civil Engineering in Kraljevo, University of Kragujevac, Dositejeva 19, 36000, Kraljevo, Serbia
[4]Faculty of Mechanical Engineering, University of Belgrade, Kraljice Marije 16, 11120, Belgrade, Serbia
[5]Faculty of Mechanical Engineering, University of Belgrade, Kraljice Marije 16, 11120, Belgrade, Serbia

Abstract

Combustion of wood logs continues to improve despite the diversification and standardization of wood-derived fuels. Gasification boilers—featuring separate gasification and combustion chambers—are widely used to meet stringent environmental requirements, yet they remain underrepresented in the engineering and scientific literature. To bridge this gap, 146 simulations were conducted to assess how refractory size, position, inclination angle, producer gas quality, and gas-inlet location affect flue-gas residence time, temperature fields, and heat transfer to boiler water. An 18-kW boiler is experimentally characterized with respect to producer-gas composition and temperature under varying gasification conditions. These data are used as boundary conditions for a CFD model that features non-premixed combustion and is described using the standard k–ε turbulence model, the Discrete Ordinates radiation model, and a domain-based weighted-sum-of-gray-gases model for radiative properties. Refractories not only protect metal surfaces, enable complete combustion, and aid particulate removal, but also enhance heat transfer. In total, 8 different combustion chamber designs are analyzed. Compared to the best refractory-free case, a combustion chamber with a U-shaped flue-gas flow path and two additional refractory-coated surfaces achieves 22% higher heat transfer despite a 17% smaller heat-exchange area. Refractories that create a U-shaped flow path extend flue-gas residence time, span at least half the chamber length, and feature an asymmetric channel height that favors a smaller flue-gas cross-section at the exit. Finally, combustion chamber design depends on upstream gasification performance—specifically, producer-gas composition and temperature, and air-preheating temperature.

Keywords: Refractory ceramic, wood-log combustion, gasification boiler, CFD modelling, heat transfer

Cite this article as: Karamarković, R. M., Novčić, Đ. A., Nikolić, M. V., Todorović, D. M., & Obradović, M. O. (2026). Impact of refractory elements design on heat transfer in the combustion chamber of wood-log gasification boilers. Journal of Thermal Engineering, 12(6), 2030–2050. https://doi.org/10.47481/jten.0082

1. Introduction

The transition toward low-carbon and renewable energy systems has significantly increased the importance of biomass as a sustainable energy source. Biomass currently accounts for approximately 8.8% of the total global primary energy supply [1], making it one of the most widely used renewable energy carriers worldwide. Within this category, fuel wood represents nearly 60% of traditional biomass consumption [2], particularly in residential and small-scale heating applications. Despite its widespread availability and relatively low processing requirements, the efficient and clean utilization of wood fuel remains a technical challenge. In conventional combustion systems, incomplete oxidation, high particulate emissions, and inefficient heat transfer are still common issues. For this reason, modern biomass boilers increasingly rely on gasification-based combustion concepts, which enable better control of the combustion process and significantly lower emissions. Gasification boilers represent the most advanced technology for wood-log combustion and currently hold an estimated 20% share of newly sold solid-fuel boilers [3]. These boilers operate with two distinct zones: a gasification chamber and

*Corresponding Author
E-mail Adress: nikolic.mi@mfkv.kg.ac.rs

Submitted: 2 February 2026; **Accepted:** 19 June 2026

This paper was recommended for publication in revised form by Editor-in-Chief Ahmet Selim Dalkılıç

a combustion chamber. In the gasification chamber, wood logs are converted into producer gas with a calorific value of 4.5-6 MJ/Nm³ using 30-60% of stoichiometric air [4]. This gas is then combusted in the combustion chamber. In small-scale boilers with a thermal capacity under 100 kW, fixed-bed gasification designs (downdraft, updraft, cross-draft), as shown in Figure 1, are dominant, with downdraft being the most common.

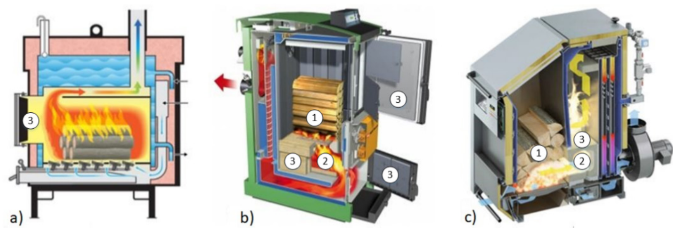

Figure 1. Multistage wood combustion. Designs with **a)** updraft, **b)** downdraft, and **c)** crossflow gasification. **1)** gasification chamber, **2)** combustion chamber, **3)** refractory elements [5]

To enhance combustion stability, separate particulates, improve heat transfer, and protect metal surfaces, refractory materials are used to shape the combustion zone [6]. These materials withstand high temperatures and corrosive environments without deformation [7]. Refractories are classified by refractoriness (1580-1770 °C, 1770-2000 °C, >2000 °C), chemical composition (oxide, non-oxide, composite) [8,9], and form (shaped bricks vs. monolithic concretes) [6,7,10,11]. Although refractory elements are widely used, their geometry and positioning are still largely based on empirical design rules rather than on systematic engineering methodologies, and their selection and configuration strongly depend on the specific combustion chamber geometry and operating conditions.

Although the performance of the gasification chamber has been extensively studied (including the effects of primary air and fuel moisture on producer gas composition [12], tar behavior [12,13], and comparisons of different biomass types [14,15]), most available data concern traditional updraft or downdraft gasification reactors [12,16,17]. Crucially, the downstream combustion chamber and its refractory elements have received far less attention. Current designs rely on empirical rules and manufacturer experience, using volumetric heat release rate as the main parameter [18-20]. The combined influence of refractory geometry (length, position, inclination) and variable producer-gas properties on heat transfer and flue-gas residence time has not been systematically quantified. This problem is exacerbated by the practical difficulty of measuring producer gas composition in situ and by its natural variability.

This study aims to bridge the identified gap by systematically quantifying the impact of both producer gas composition and refractory element design on heat transfer and combustion chamber performance. To achieve this, an 18kW wood-log gasification boiler was investigated experimentally to determine the producer gas composition, gas temperature, and tar content under realistic operating conditions.

The experimentally obtained data were used as boundary conditions for a validated Computational Fluid Dynamics (CFD) model of the combustion chamber. A comprehensive parametric study covering 146 configurations was conducted, varying refractory ceramic length, position, and inclination angle, as well as producer-gas inlet location. The response variables evaluated were flue-gas residence time, temperature fields, and heat transfer to boiler water.

The obtained results establish quantitative design guidelines for optimizing refractory configurations and enhancing the thermal performance of biomass gasification boilers. Their applicability is not limited to the investigated case study because energy density is a fundamental parameter in combustion chamber sizing. Consequently, the findings can be extended to similar boiler designs across a broad range of thermal capacities.

2. Experimental investigations

Experimental investigations were conducted on a wood-log gasification boiler with a nominal thermal power of 18-kW. The main components of the boiler are a gasification chamber (410×520×700 mm), a combustion chamber, and a convective section (Figures 2 and 3b). The gasification chamber simultaneously serves as fuel storage. Preheated primary air is added through inlets located on the side walls of the chamber at a height of 150 mm above its bottom, and the producer gas is combusted in the zone between the gasification and combustion chambers. The refractory plate (3 in Figure 3b), located between the gasification and combustion zones, supports the gasified fuel bed, provides heat for endothermic reactions, and channels combustion air. The other refractory element (5 in Figures 2 and 3b), together with the plate, forms a combustion zone for the producer gas and serves to ensure as complete as possible combustion of the producer gas laden with particulates, to facilitate the removal of ash through the cleaning doors, to enhance heat transfer within the combustion chamber, and, through a combination of velocity changes and inertial forces, to promote particle deposition. Apart from these refractory elements and the door, the chamber is largely surrounded by channels through which the water flows. The convective section of the boiler (6 in Figure 2) consists of three parallel pipes, each with an inner diameter of 82.5 mm and equipped with a wire-coil turbulator. The fan (7 in Figure 2) creates a slightly negative pressure inside the boiler, which is automatically regulated by two valves and the exhaust fan. The primary air valve, in combination with the variable-speed fan, attempts to achieve the desired thermal output, whereas the secondary valve maintains a constant oxygen concentration in the flue gas, typically targeted at 7%. The boiler is designed to provide near-constant thermal power and to couple with a buffer tank, but variations in downdraft gasification and in water inlet temperature lead to quasi-steady-state operation. Unsteadiness in the gasifier is primarily caused by its batch-type operation, bridging in the fuel bed, and the fuel's variable moisture content.

2.1. Fuel properties

For experimental investigations, beech wood was used as the test fuel. Table 1 shows its proximate and ultimate analyses, lower heating value (LHV), and applied measurement standards.

Table 1. Proximate and ultimate analysis of the fuel. **1)** on a dry basis, **2)** as ash, **3)** on a dry ash-free basis, **4)** average value

Volatile matter[1]	Ash[1]	Fixed carbon[1,2]	C[3]	H[3]	O[3,2]	N[3]	S[3]	W[4]	LHV kJ/kg
ISO 18123	ISO 18122	calc.	ISO 16948		calc.	ISO 16948	ISO 16994	ISO 18134	ISO 18125
85.9	0.57	13.4	49.1	5.7	44.5	0.15	0.045	12.85	14540

After three years of natural drying, the beech wood used for testing was exceptionally dry. Manufacturers typically require the moisture content to fall within the range of 15 wt% to 20 wt%, though some even recommend a broader upper limit of 25 wt%. Compared with wood density and chemical composition, moisture content is the most significant factor influencing the combustion quality of wood logs. This implies that the findings of this analysis are applicable to wood logs combusted in gasification boilers, provided the wood is naturally well-dried to within the recommended moisture content ranges and irrespective of species or density.

2.2. Measured quantities and measurement procedure

In the examined boiler, in-situ measurements in the gasification chamber are not feasible because water flow channels occupy most of the chamber volume, imposing spatial limitations. To obtain a more realistic simulation of operating conditions, the measurements were carried out cyclically: after every 25 minutes of operation, the chamber was investigated during a 10-minute interval. During sampling, the fan (7 in Figure 2) operated at a constant rotational speed, while the primary air flow rate was maintained at an approximately constant level by a manual control valve (16 in Figures 2 and 3a). Despite continuous variations in flow resistance within the chamber, the air flow rate was maintained within ±0.1 l/s using the control valve. This valve is necessary because closing the secondary air supply (3 in Figure 2) disturbs the flow pattern in the boiler and increases the flow rate through the gasification chamber by closing the parallel secondary air branch. A volumetric flow meter (15 in Figures 2 and 3a) and the aforementioned control valve were used at this measurement location. To ensure measurement accuracy, both the flow meter and the control valve were installed on a straight pipe section with a minimum upstream length of 5D from the nearest local flow disturbance. The primary air mass flow rate was calculated based on the measured ambient air temperature and humidity (measurement point 4 in Figure 2 and Table 2).

After the secondary air supply was closed, gas sampling and temperature measurement probes were installed at sampling point 2 (Figures 2 and 3b). A K-type thermocouple was positioned adjacent to the gas sampling probe and housed in a stainless-steel tube, which served as a barrier against thermal radiation from the surrounding ceramics. Gas sampling was performed using a water-cooled probe (1 in Figure 2), with cooling water supplied at approximately 12 °C (2) and discharged at position 3. The probe was slightly inclined toward a condenser cooled with ice water at 0 °C (4 in Figure 2). The cooled gas was then directed from the condenser to gas-washing bottle 5 (Figure 2), which had a volume of 0.25 dm^3 and contained 0.15 dm^3 of isopropanol. The washing bottle was immersed in ice water at 0 °C throughout the entire procedure. The main portion of the moisture and tar was separated from the gas in the condenser. Figure 4a, taken during the measurements, shows the collected condensate, which represents a mixture of water, tar, and solid particles. The latter predominantly consists of ungratified carbon entrained in the gas flow. In study [21], Hasler and Nussbaumer presented an absorption-based method for sampling and separating tar from producer gas. Using this method, Buchmayr et al. [12] sampled tar from gas produced by the gasification of wood chips in a small-scale boiler. Unlike study [12], in which two water-filled and five isopropanol-filled washing bottles were used(three of which were placed in a vessel maintained at −10 °C),in the presented measurement, considering its specific objectives, required accuracy, the use of a water-cooled probe, and a large condenser, only a single washing bottle was employed.

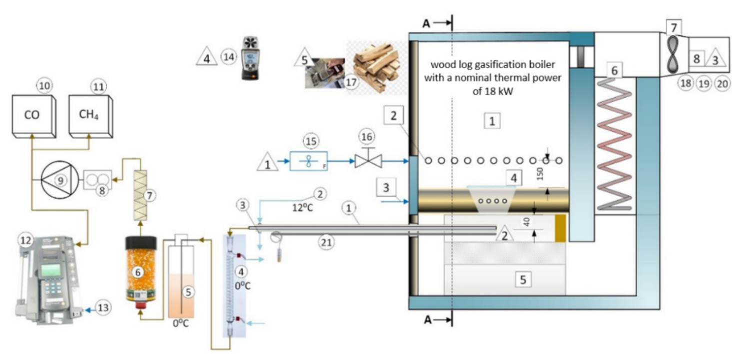

Figure 2. Experimental set-up. In squares: **1)** gasification chamber, **2)** primary air inlets, **3)** secondary air, **4)** gasification chamber outlet (secondary air inlet), **5)** refractory brick in the combustion zone, **6)** convective section of the boiler with wire coil turbulators. Measurement points shown by triangles: **1)** primary (gasification) air, **2)** gas sampling and temperature measurement, **3)** measurement of flue gas characteristics at the boiler outlet, **4)** ambient conditions, **5)** moisture content of the wood logs. Measuring equipment indicated by circles: **1)** gas sampling probe, **2,3)** cooling water inlet and outlet of the probe, **4)** condenser, **5)** washing bottle filled with isopropanol, **6)** silica gel filter, **7)** glass fiber filter, **8)** dry gas flow meter, **9)** vacuum pump, **10) CO measurement, 11)** CH4 measurement, **12)** gas analyzer, **13)** gas dilution air, **14)** anemometer, **15)** flow meter, **16)** manual control valve, **17)** wood moisture meter, **18)** temperature and O_2 sensors in the flue gas, **19)** temperature measurement, **20)** isokinetic particle sampling, **21)** producer gas temperature [5]

Downstream of the washing bottle, which was used to remove remaining moisture and particles, silica gel filters (6 in Figure 2) and glass-fiber filters (7 in Figure 2) were employed. After the filters, the volumetric flow rate and temperature of the sampled gas were measured using a Zambeli ZB1 device (Tab. 2). The dry producer gas was then split into three lines: two were directed to automatic gas analyzers for measuring high concentrations of CH_4 and CO (Tab. 2), and the third was routed to a Testo 350 XL gas analyzer (12 in Figure 2). These devices (10 to 12) are equipped with their own vacuum pumps, which have been omitted from Figure 2 for clarity. Using the gas analyzer, the dry fuel gas was diluted with ambient air by a factor of 40 (ratio 1:39), and the concentrations of O_2, CO_2, and CO were measured. The N_2 concentration was calculated based on the primary air flow (15 in Figure 2) and the ultimate composition of the beech logs. As in the study by Buchmayr et al. [12], it was assumed that all tar was in the form of heptane(C_7H_{16}).The H_2 concentration was determined under the assumption that in the dry gas, after removal of moisture and tar, no components other than CO, CO_2, CH_4, O_2, and N_2 were present.

At the measurement point 3 (Figure 2 and Table 2), flue gas temperature and O_2 concentration was continuously checked by the boiler control system (19). Prior to the measurements described above, boiler performance tests by EN 303-5 were conducted at the same measurement point (see Table 3). The gas temperature within the sampling line was controlled at the volumetric flow measurement location (8 in Figure 2).

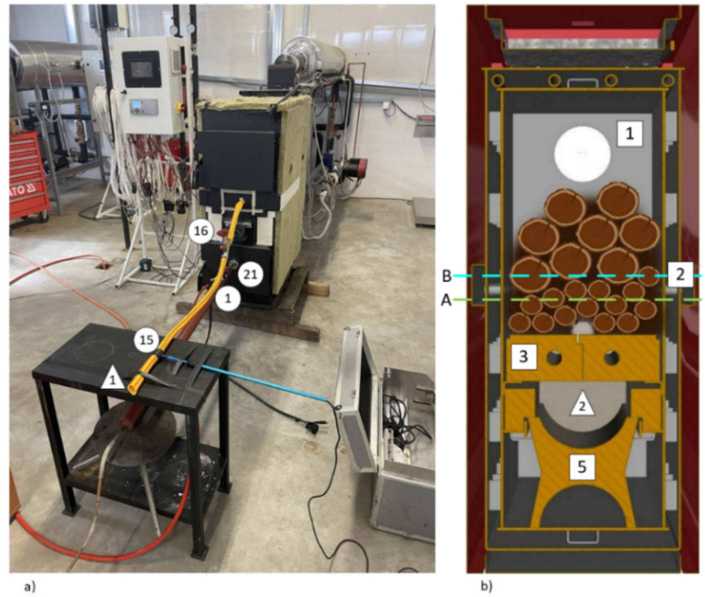

Figure 3. a) The tested boiler with part of the measuring equipment, **b)** Cross-sectional view of the boiler through the gasification chamber (labels correspond to those in Figure 2) [5]

Table 2. Measuring points, quantities and characteristics of the applied measuring equipment

MP	Number	Quantity and device	Error (abs. or rel.)
1	15	Primary air volumetric flow meter Flowatch, measuring range 1 – 30 m/s, ∅20 mm, resolution 0.1 m/s, 3 cm/s, operating temperature – 50 to 100 °C	±2% FS
2	8	Volumetric flow rate of the producer gas – Zambeli ZB1 – min 16 dm^3/h, maximum flow rate 4 m^3/h	±3%
2	10	CO concentration in dry producer gas. Gas analyzer Uras 3E (manufacturer Hartmann & Braun). Measurement range: 0-25% CH_4, 0-50% CH_4	±1%
2	11	CH_4 concentration in dry producer gas. Gas analyzer Uras 3E (manufacturer Hartmann & Braun). Measurement range: 0-10% CO, 0-40% CO	±1%
2	12	CO concentration in dry producer gas	±5%
2	12	CO_2 concentration in dry producer gas	±0.3 vol%+1
2	12	O_2 concentration in gas	±0.8%
2	4,5	Moisture and tar content in dry producer gas – determined by the gravimetric method using JEX-200	±0.2 mg
2	21	Temperature of dry producer gas at the outlet of the gasification chamber – Type K thermocouple (NiCr-Ni) max. 1370 °C	±1 °C
3	18	Flue gas temperature and oxygen concentration – monitored by the boiler control system	±1 °C ±0.1 vol%
3	19,20	Volumetric composition and particulate matter content in the flue gas – Horiba ENDA 5000	O_2±0.8%, CO±10 ppm, NO_X±5%, SO_2 ±10 ppm
4	14	Ambient air temperature and relative humidity	relative humidity ±2.5% rH temperature ±0.5 °C
5	17	Wood moisture – Testo 616 (<50% moisture), resolution 0.1%	rel.=0.1%/DB%

Table 3 presents the main technical specifications for the tested gasification boiler. Except for excess air (which is always within the reported range) and primary air, other data and their corresponding uncertainties were taken from official testing performed by a certified company according to EN 303-5. In this type of boiler, the control system regulates the secondary air flow so that the oxygen content in the flue gas is approximately 7% or, alternatively, is set to another value that ensures high efficiency with the lowest possible emissions. Consequently, the most common air excess ratio is around 1.5. In most cases, the primary air, expressed as the excess air ratio, ranged from 0.35 to 0.45. The uncertainties in the excess air are calculated based on the relative errors in the determination of actual air (2%, see Tab. 1) and stoichiometric air (3.5%).

Table 3. Technical data of the tested boiler

Nominal power	18.07 ± 0.08 kW
Efficiency	90.3 ± 0.81%
CO emission (corrected to 10% O_2 in dry flue gas)	126.57 ± 1,70 mg/Nm^3
NOX emission (10% O_2)	175.75 ± 2.6 mg/Nm^3
OGC emission (10% O_2)	5.02 ± 0.22 mg/Nm^3
Particulate matter emission (10% O_2)	18.44 ± 0.55 mg/Nm^3
λ – most common	1.5÷1.6 (± 0.06)
λ primary air (during testing)	0.22÷0.67 (min÷max), (average 0.39± 0.02)

Table 4 presents the results of four testing sessions. The last two columns show the composition of producer gases at the optimal gasification points for beech wood with 12.85 % moisture, under a pressure of 0.1 MPa. CBP – SRC denotes optimal gasification with air at standard reference conditions [22], while CBP – PA represents optimal gasification with air preheated to the gasification temperature [23]. The optimal point is also referred to as the carbon boundary point [24]. At this stage, the gasification process is described as a chemical evaporation process in which the minimum amount of air required to convert all carbon into the gaseous phase is added. Under these conditions, the gas retains the maximum amount of chemical energy from the original biomass. Compared to the values and experimental results reported in [12] and [15], unexpected gas compositions were measured. Column 1 shows the gas obtained at the start of the tests, when the boiler was filled with fuel to a level below the primary air inlet (line A–A in Figure 3b). In this case, the boiler was unable to reach its nominal thermal power. Subsequently, the fuel level in the chamber was raised to the height corresponding to the line B–B in Figure 3b. The obtained values are shown in columns 2–4. Column 3 corresponds to the most frequently obtained gas composition. These are average values; their variation during sampling is illustrated in Figure 4b.

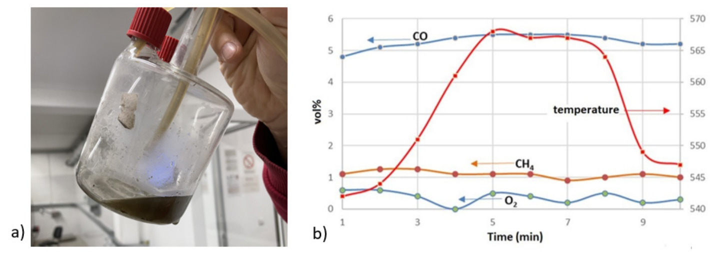

Figure 4. a) collected condensate (mixture of water, tar and solid particles), **b)** changes in the volumetric concentrations of CO, CH_4, O_2 and flue gas temperature during Test 3 [5]

Figure 4b shows the average-minute values obtained as the mean of four measurements taken during a one-minute sampling interval. In Figure 4b, relatively small variations in the results can be observed within a single measurement session. The masses of moisture and tar, determined using the described gravimetric method, indicate that the tar content in the producer gas is relatively high. Tar was the main contributor to the gas heating value. The amounts of H_2O and tar in the gas were measured for all testing sessions and subsequently allocated to individual gas compositions, assuming that the same quantities of H_2O and tar were emitted during each session. The obtained moisture-to-tar ratio is consistent with the values reported in [12] for an air excess ratio of 0.25. The same study demonstrated that the tar content decreases with increasing primary air supply, while the gas temperature at the chamber outlet generally increases with higher airflow. The obtained results are similar to the theoretical values reported in [17], but differ in terms of significantly lower gas temperature and increased tar content. This is also influenced by the gasification chamber being largely surrounded by water channels, thereby reducing gas temperature and altering its composition.

Table 4. Obtained experimental and theoretical model results

Test	1	2	3	4	CBP - SRC	CBP - PA
λ	0.28 ± 0.01	0.43 ± 0.02	0.30 ± 0.01	0.28 ± 0.01	0.285	0.239
CO %	2.4 ± 0.19	4.1 ± 0.20	5.3 ± 0.21	5.4 ± 0.21	22.2	26.2
CO_2 %	19.5 ± 0.25	14.7 ± 0.25	15.7 ± 0.25	17.2 ± 0.25	10.3	8.4
CH_4 %	0.3 ± 0.009	1.0 ± 0.013	1.1 ± 0.014	1.3 ± 0.016	1.3	1.3
H_2 %	0.2 ± 1.1	1.1 ± 1.3	1.1 ± 1.2	1.2 ± 1.1	22.8	25.5
H_2O %	22 ± 0.43	15.5 ± 0.29	18.2 ± 0.34	20.0 ± 0.39	5.4	4.6
N_2 %	55.2 ± 1.1	62.8 ± 1.3	58.1 ± 1.2	54.5 ± 1.1	38.0	34

O_2 %	0.3 ± 0.04	0.6 ± 0.04	0.5 ± 0.04	0.4 ± 0.04	0.0	0.0
LHW MJ/$kg_{biomass}$	0.69 ± 0.28	2.25 ± 0.32	2.21 ± 0.30	2.14 ± 0.28	12.64	13.53
LHW including tar MJ/$kg_{biomass}$	11.5 ± 3.25	11.5 ± 3.39	11.5 ± 3.13	11.1±3.12		
Moisture mass kg/$m^3_{dry\_producer\_gas}$	0.152 ± 0.003					
Tar mass kg/$m^3_{dry\_producer\_gas}$	0.109 ± 0.032					
$T_{producer\_gas}$ °C	497 ± 1	618 ± 1	556 ± 1	570 ± 1	674.5	698.6

In the first test series (Tab. 4), low values of combustible components are due to a thin layer of gasified biomass and the formation of channels (the interstitial voids within the wood-log fuel bed). In this case, nearly complete combustion occurs in the channels, which represent a form of fluid short circuit for the airflow and, subsequently, the gas flow. Smaller amounts of air pass through the remaining part of the fuel bed, causing gasification of the biomass. Fuel devolatilization, which results in tar formation, depends on the rate at which the heat flux spreads from the interstitial voids within the wood-log fuel bed to the remaining fuel.

The gas temperature at the outlet of the gasification chamber did not exhibit significant oscillations during the sampling period (see range in Figure 4), and was generally higher when more primary air was supplied. More air releases more energy during oxidation reactions, resulting in increased gas temperature. The measured values were lower than those corresponding to the optimal gasification point, due to heat losses to the boiler water, secondary air, and the surroundings, and are consistent with the results reported in [12]. Anomalies observed during tests with smaller fuel loads were caused by the formation of the interstitial void space within the wood-log fuel bed, as previously mentioned. These channels disappear after several fuel batches as a result of fuel fragmentation induced by shrinkage and thermal degradation, as described in more detail in [13].

Table 4 presents the standard uncertainties for the measured and calculated product gas components and properties. These uncertainties are derived from the data in Table 2 and from the results of the wood analysis. Most gas species, CO, CO_2, CH_4, O_2, N_2, and H_2O, have acceptable standard uncertainties. Because its low concentration and it is determined by subtracting the volume fractions of the other gas species, the hydrogen volume fraction in the producer gas exhibits a substantial standard uncertainty. The 2% uncertainty associated with the high volume fraction of nitrogen is the predominant contributor to this uncertainty. This effect, together with a substantial standard uncertainty for tar (29.7%), leads to relatively high uncertainties in the LHVs. Nevertheless, because most gaseous species have low uncertainties and the energy balance of the boiler agrees with the presented values, these data are used as input for the CFD model of the combustion chamber.

3. The CFD model

The commercially available ANSYS software and its integrated module FLUENT 18.1 [25] were employed for the numerical simulation of the producer gas combustion within the combustion chamber. The simulations were performed based on the defined geometry, generated computational mesh, and boundary conditions. Different turbulence models [26,27] were preliminarily tested to assess their impact on the simulation results. Among the tested models, the Standard k–ε turbulence model [28,29] provided results that were in the closest agreement with the experimental measurements (see Appendix B). For this reason, the standard k–ε model was selected for the final simulations. In developing the non-premixed combustion model, the energy equation was solved, the selected standard k–ε turbulence model was adopted, and the discrete ordinates (DO) radiation model was applied. The non-premixed combustion model in ANSYS Fluent is based on the mixture fraction/PDF approach. In this model, the thermo-chemical state of the reacting mixture is described by the mixture fraction and its variance, while turbulence–chemistry interaction is accounted for using a presumed probability density function (PDF). The chemical-state relation was defined using the chemical-equilibrium option, such that species composition and temperature are obtained from equilibrium calculations as functions of the mixture fraction. Therefore, the combustion process is represented using an equilibrium flamelet approach. The oxidation of the main fuel species (CO, H_2, CH_4, and tar compounds) is determined by equilibrium chemistry incorporated into the flamelet library. The DO radiation model, which solves the radiative transfer equation for a finite number of discrete directions, is well suited and frequently recommended for combustion simulations where high solution accuracy is required [30]. For radiation modeling, the WSGGM-domain-based approach was employed to determine the absorption coefficient. Figure 5a illustrates the CFD model of the combustion chamber of the investigated wood-log gasification boiler.

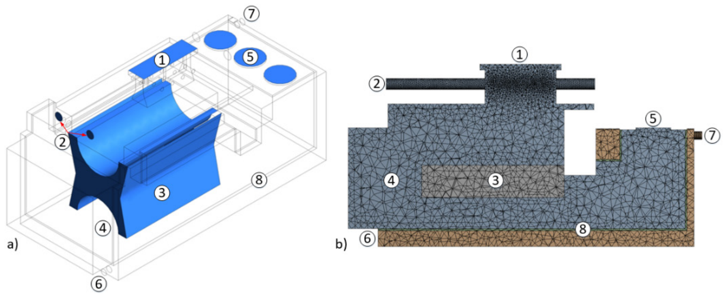

Figure 5. a) CFD model of the combustion chamber of the investigated wood gasification boiler, **b)** The computational mesh represented by a cross-section of the combustion chamber. **1)** producer gas inlet, **2)** combustion air inlet, **3)** refractory ceramics, **4)** combustion chamber, **5)** flue gas inlet into a tubular heat exchanger that consists of three parallel pipes, **6)** boiler water inlet, **7)** boiler water outlet, **8)** boiler steel plate.

Figure 5b illustrates the computational mesh represented by a cross-section of the combustion chamber. The mesh consists of 55547 nodes and 275310 elements. The minimum length of a side of an element is 0.538 mm, whereas the maximum length is 20 mm. The mesh quality is considered satisfactory, as the average values of y-plus, element quality, aspect ratio, orthogonal quality, and skewness fall within acceptable limits, amounting to 31.9, 0.814, 1.97, 0.741, and 0.258, respectively [31,32].

The numerical discretization schemes used in the present simulations were as follows. The pressure equation was solved using the PRESTO! scheme, while the momentum, turbulent kinetic energy (k), turbulent dissipation rate (ε), energy, Discrete Ordinates (DO) radiation, mean mixture fraction, and mixture fraction variance equations were discretized using second-order upwind schemes. The gradient terms were evaluated using a least-squares cell-based method, and the cell-face fluxes in the solver were treated using the SIMPLE pressure-velocity coupling algorithm. Under-relaxation factors for all solved variables were set to 0.3, providing stable convergence throughout the simulations. Residual targets of 10^{-6} for energy and 10^{-5} for do-intensity were used.

3.1. Boundary conditions

The inlet to the combustion chamber was defined as a producer-gas inlet boundary, with the producer gas flow specified as a mass flow rate, uniformly distributed across the cross-sectional area (1 in Figure 5). The combustion air inlets to the combustion chamber are defined at two locations, each specified with an inlet boundary condition at which the combustion air flow is prescribed as a mass flow rate uniformly distributed over the corresponding cross-section (2 in Figure 5). The flue gas outlet from the combustion chamber (which effectively corresponds to the flue gas inlet to the tubular heat exchanger shown as 5 in Figure 5) was defined as an outlet-type boundary. The boundary condition was specified by selecting the static pressure option and setting a relative pressure of 0 Pa. The boiler water inlet was defined as an inlet boundary, with the water flow specified as a mass flow rate, uniformly distributed across the cross-section (6 in Figure 5). The water outlet (7 in Figure 5) was defined as an outlet boundary, where the boundary condition was set by selecting the static pressure option and assigning a relative pressure of 0 Pa. All remaining surfaces were assigned wall boundary conditions. Under real operating conditions, heat losses through the doors are approximately 400 W/m². However, due to the small area of the doors and the right-hand closed surface in the flame zone, which together total 0.13 m², the resulting heat losses are negligible, at approximately 52 W. Therefore, the doors and the right-hand closed surface in the flame zone were modeled as adiabatic. Table 5 presents the boundary conditions used in the numerical simulations. As previously noted, all tar was assumed to be in the form of heptane (C_7H_{16}). The parameters used in the numerical simulations for the refractory ceramics (corundum 90) were taken from [33] and are as follows: λ=2.33 W/mK, Cp=1.118 kJ/kgK, and ρ=2.83 g/cm3. Like any refractory material, this material has pros and cons: good wear and abrasion resistance required in this case (Figures 2, 3, 5, 6), high volume stability (low creep), and high thermal conductivity, but also high vulnerability to alkali attack and poor thermal shock resistance [34-36]. To balance these pros and cons, modern boiler designs rarely use pure corundum 90 but rather corundum–mullite composites that improve thermal shock resistance, or versions blended with chromium oxide or silicon carbide to block pores and prevent alkali vapor penetration [37].

Table 5. Boundary conditions used in the numerical simulations

Test	1	2	3	4	CBP-SRC	CBP-PA
CO %	2.344	4.004	5.176	5.273	22.2	26.2
CO_2 %	19.043	14.355	15.332	16.797	10.3	8.4
CH_4 %	0.293	0.977	1.074	1.27	1.3	1.3
H_2 %	0.195	1.074	1.074	1.172	22.8	25.5
H_2O %	21.484	15.137	17.773	19.531	5.4	4.6
N_2 %	53.906	61.328	56.738	53.223	38	34
O_2 %	0.293	0.586	0.488	0.391	0	0
C_7H_{16} %	2.442	2.539	2.345	2.343	0	0
$_{producer\_gas}$ kg/s	0.00373	0.00385	0.00373	0.00357	0.00322	0.00291

$T_{producer\_gas}$ °C	497	618	556	570	674.5	698.6
$_{combustion\_air}$ kg/s	0.00713	0.00834	0.00784	0.00763	0.00724	0.00774
$T_{combustion\_air}$ °C	300	300	300	300	300	300
$_{boiler\_water}$ kg/s	0.2	0.2	0.2	0.2	0.2	0.2
T_{boiler_water} °C	55	55	55	55	55	55

The surface emissivity values used in the radiation model were adopted from the literature. The emissivity of the refractory ceramic and steel surfaces was set to ε = 0.9 and ε = 0.8, respectively, based on data reported in [38,39]. In the present simulations, all emissivity values were assumed to be constant and independent of temperature.

Soot and particulate matter are neglected in the model because they have dual effects on heat transfer in the combustion chamber that cancel each other out. Namely, they enhance heat transfer when suspended in the flame [40] but inhibit it when deposited, in this case particularly on the bottom surface.

3.2. Validation of the CFD model

The CFD simulation results were compared with in-situ measurements of the same boiler [41], focusing on the flue gas temperature at the inlet of the tubular heat exchanger that consists of three parallel pipes, with the temperature measured at the central pipe (5 in Figure 5). The simulation was performed on a PC workstation equipped with an AMD Ryzen 5 7500F processor (6 cores, 12 threads, 3.70 GHz), 64 GB of RAM, and an AMD Radeon RX 7800 XT graphics card. During the simulation, an average of 32 GB of RAM was utilized, while the CPU operated at full capacity. Figure 6 illustrates the results of the CFD simulation, showing the temperature field within the flue gas domain. The flue gas temperature obtained from the CFD simulation (324.5 °C) was compared with the experimental value (297.8 °C) reported at the boiler thermal output of 18.11 kW in Tab. 4 in [41], yielding a deviation of nearly 9%. However, because radiative heat transfer, which depends on absolute temperature, is dominant inside the combustion chamber, the deviation becomes 4.7%. This is satisfactory, as the discrepancy can also be influenced by the inherently unsteady (quasi-steady-state) boiler operation (explained in Section 2), measurement uncertainties (flue gas composition, Tab. 2 in [41]; boiler capacity: 18.11 kW ± 0.38% [41]; and the reported efficiency: 90.3% ± 0.81%), and simplifications in the model development. The main simplification is that the model neglects heat loss through the front door, which could lead to overestimation. The value of 297.8 °C [41] used for comparison is an average obtained over a 23-minute interval. As the boiler operates in a quasi-steady-state manner, the variation of this temperature is depicted in [41].

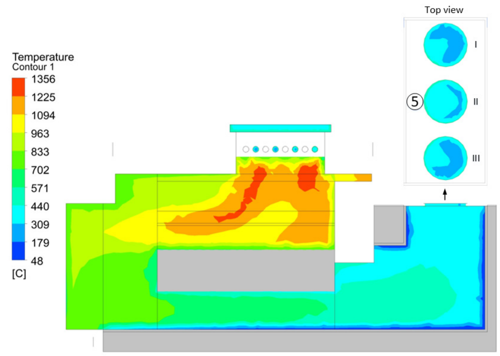

Figure 6. Flue gas temperature field (a cross-section of the combustion chamber and a top view of three parallel pipes)

4. Proposed new technical design

This section presents the investigated combustion chamber configurations for producer gas combustion in wood-log gasification boilers. The optimal size and positioning of the refractory ceramics and the location of the producer gas inlet were determined using a boiler with a nominal thermal power of 18-kW as a reference case. Based on the combustion chamber volume of 0.083 m3 (calculated from the proposed dimensions of 900×303×303 mm) and a boiler thermal power of 18-kW, the heat transfer rate from the flue gas to the boiler water per unit volume of the combustion chamber was determined to be 216 W/m³. In engineering practice, this parameter is of particular importance for the design of combustion chambers. Compared with values characteristic of log wood gasification boilers with thermal powers of 18, 25, 26, and 30-kW [42-44], which range from 208 to 225 W/m³, the differences are negligible. This comparison confirms that the proposed combustion chamber volume is appropriate for the specified boiler thermal power. In the subsequent section of the paper, the influence of different configurations of refractory ceramics on heat transfer from the flue gas to the boiler water was examined. Figure 7 illustrates the 3D model of the proposed combustion chamber design for a wood-log gasification boiler. The CFD simulations were performed using the methodology described in Section 3.

4.1. Influence of refractory ceramic length and producer gas inlet position on heat transfer

The goal was to determine the optimal size of the refractory ceramic and position of the producer gas inlet in the combustion chamber. A total of 25 combinations were analyzed, comprising five different lengths of the refractory ceramic and five different positions of the producer gas inlet, as shown in Tab. 6. The position of the producer gas inlet is denoted by the symbol p, while the length of the refractory ceramic is denoted by the symbol l. The individual configurations are labeled in the form pili, where the index i ranges from 1 to 5, starting from p_1l_1, p_1l_2, … up to p_5l_5. Figure 8a illustrates the two dimensions that define the examined designs. The design is characterized by a U-shaped flow path within the combustion chamber.

Table 6. Combinations pili used in the numerical simulations

Producer gas inlet position (p_i)	Refractory ceramic length (l_i)
p_1=150 mm	l_1=300 mm
p_2=250 mm	l_2=375 mm
p_3=350 mm	l_3=450 mm
p_4=450 mm	l_4=525 mm
p_5=550 mm	l_5=600 mm

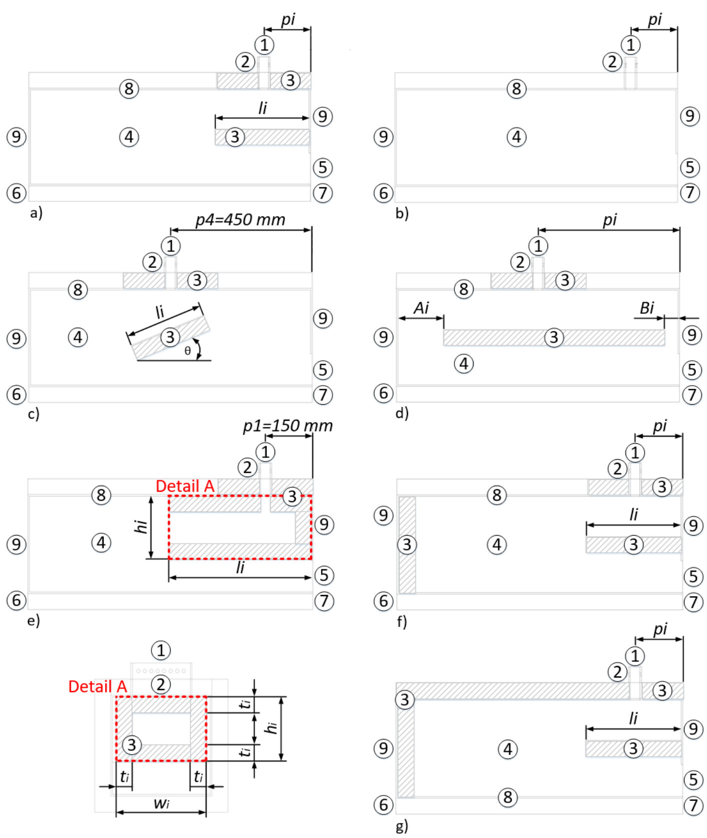

Figure 8. Examined combustion chamber designs. **1)** producer gas inlet, **2)** combustion air inlet, **3)** refractory ceramic, **4)** fluid domain, **5)** flue gas outlet, **6)** boiler water inlet, **7)** boiler water outlet, **8)** boiler steel plate, **9)** adiabatic wall

Figure 9 shows the results obtained from the numerical simulations of the design illustrated in Figure 8a. The set convergence criterion ($< 1\times10^{-4}$) was met shortly before the 13000th iteration, corresponding to a total computational time of approximately 35 minutes. Figure 9 presents the total and radiative heat transfer from the flue gas to the boiler water. In all examined cases, the total energy input into the combustion chamber is the same. Based on the simulation results, it can be concluded that the most favorable effect on heat transfer is achieved for configurations in which the producer gas inlet is positioned closest to the flue gas outlet and the refractory ceramic has a minimum length of approximately half the chamber length (configurations p_1l_3, p_1l_4, and p_1l_5, highlighted in gold). This can be explained by the longer refractory ceramic, which directly lengthens the flow path and consequently increases the residence time of flue gases within the firebox. The total heat transferred from the flue gas to the boiler water shows minimal variation among these three configurations, ranging from 13329 to 13498 W. The least favorable configurations can also be observed in Figure 9 (highlighted in green) and are denoted as p_2l_1, p_3l_1, p_3l_2, and p_4l_3. This indicates that the heat transfer decreases as producer gas inlet approaches the boiler water inlet. As in the previous case, the total heat transferred among these configurations shows minimal variation, ranging from 10912 to 10990 W. Consequently, the difference between the most and least favorable configurations amounts to approximately 2.5 kW.

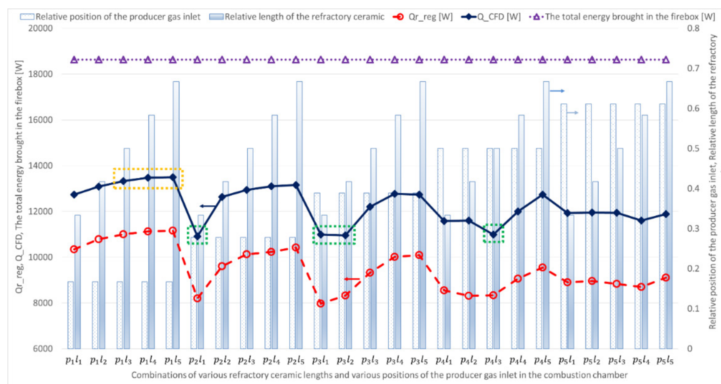

Figure 9. Influence of the length and producer gas inlet position on heat transfer for ceramic elements that create a U-shaped flue gas flow path

In Figure 9, the radiative heat transfer from the flue gas to the boiler water is indicated by the red dashed line. These values were also obtained from CFD simulations and can be read on the left ordinate. Regression analysis was used to interpret the results. All regressions were performed using the ordinary least squares (OLS) method. The data used consist of 146 CFD simulation runs covering the full range of operating conditions described in Section 3. No cross-validation was performed, as the primary objective was to obtain the best possible fit to the available CFD data; however, detailed fit statistics were provided to assess model quality. Although the use of nondimensional groups (e.g., Biot-like numbers or Stefan–Boltzmann scaling) is often desirable for enhancing the physical interpretability and generality of correlations, their introduction in the present study did not yield satisfactory statistical performance. Several alternative formulations incorporating physically motivated dimensionless parameters were tested, but they consistently resulted in lower R^2 and higher RMSE compared to the polynomial expressions reported here. This outcome highlights a well-known characteristic of regression-based modeling: a model can provide excellent predictive capability even if its individual terms lack direct physical meaning. The strength of ordinary least squares regression lies in its ability to capture complex relationships purely from data, making it a valuable tool for interpolation within the calibrated range. Therefore, while the final equations (Eqs. 1–8) are empirical, their high accuracy (as evidenced by the fit statistics in Table 1) justifies their use for the intended purpose. Future work may explore hybrid approaches that combine physical principles with data-driven techniques to further improve both interpretability and predictive performance. In all regression equations considered, temperature is expressed in degrees Celsius. Although radiative transfer is fundamentally dependent on absolute temperature (given its proportionality to the fourth power of temperature), the choice of temperature scale in the proposed formulations does not influence the result. This is because temperature appears in the equations exclusively as a dimensionless ratio or a temperature difference, thereby neutralizing the effect of the absolute scale. Consequently, the equations are invariant under linear transformations of the temperature scale, rendering conversion to absolute units unnecessary.

By applying regression analysis in MS Excel [45], a mathematical equation describing the heat transferred by radiation, in watts, from the flue gas to the boiler water was obtained, which is expressed as follows:

$$
\begin{aligned}
Q_{r\_reg} &= c_0 + c_1 \cdot p_r + c_2 \cdot l_r + c_3 \cdot \left(\frac{p_r}{l_r}\right)^2 + c_4 \cdot \left(\frac{\Delta T_{gas}}{\Delta T_{water}}\right)^2 \\
&+ c_5 \cdot (\Delta T_{gas} - \Delta T_{water})^2 + c_6 \cdot \left(\frac{T_{gas_{mean}}}{T_{water_{mean}}}\right)^2 + c_7 \cdot \left(\frac{p_r}{l_r}\right)^3 \\
&+ c_8 \cdot \left(\frac{\Delta T_{gas}}{\Delta T_{water}}\right)^3 + c_9 \cdot \left(\frac{T_{gas_{mean}}}{T_{water_{mean}}}\right)^3 + c_{10} \cdot \left(\frac{p_r}{l_r}\right)^4 \\
&+ c_{11} \cdot \left(\frac{\Delta T_{gas}}{\Delta T_{water}}\right)^4 + c_{12} \cdot \left(\frac{T_{gas_{mean}}}{T_{water_{mean}}}\right)^4 \qquad (1)
\end{aligned}
$$

Where c_i are the constants listed in Tab. 7, $p_r = p_i/L$ is the relative position of the fuel gas inlet, $l_r = l_i/L$ is the relative length of the refractory ceramic, with L=900 mm being the length of the combustion chamber. ΔT_{gas} denotes the temperature difference between the producer gas at the chamber inlet and the flue gas at the chamber outlet, ΔT_{water} is the temperature difference of the water between inlet and outlet, $T_{gas\ mean}$ is the mean flue gas temperature, and $T_{water\ mean}$ is the mean boiler water temperature.

Table 7. Constants used in equation 1

c_0	c_1	c_2	c_3	c_4	c_5	c_6
322834.99	3644.1	-399.67	-8198.92	15.55	0.215	-267997.93
c_7	c_8	c_9	c_{10}	c_{11}	c_{12}	
8131.51	-26.1	133772.72	-2197.23	3.465	-18662.94	

Configuration p_1l_3 was selected as optimal for two reasons. The first reason is the previously noted negligible difference in total heat transfer from the flue gas to the boiler water, compared with other favorable configurations (Figure 9). The second reason relates to the length of the refractory ceramic and the associated potential for material savings when this configuration is adopted. Figure 10a presents the results of the numerical simulation for the optimal configuration, with particular emphasis placed on the temperature field of the flue gas. The flue gas temperatures at the outlet of the combustion chamber ranged from 425 to 549 °C. The simulation results indicate that an extended flow path, i.e., a prolonged residence time of the flue gases within the combustion chamber most favorably affects heat transfer. The primary function of the refractory ceramic is to separate the gas inlet from the gas outlet. However, from a heat transfer perspective, positioning the ceramic closer to the outlet side is more advantageous, as it promotes convective heat transfer and enhances radiative heat exchange from hotter to cooler regions. Furthermore, the simulations showed that the water temperature increases on average by 9 to 20 °C during heat exchange within the combustion chamber. Figure 10b illustrates the p_4l_3 configuration, which has an unfavorable effect on the heat transfer. In this configuration, distinct colder zones, which result from the more distant position of the producer-gas inlet, can be clearly identified.

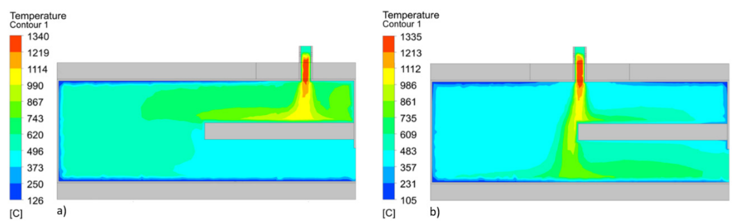

Figure 10. Results of CFD simulations for ceramic elements that create a U-shaped flue gas flow path. **a)** the best configuration p_1l_3, **b)** the least favorable configuration p_4l_3

4.2. Influence of the producer gas inlet position on heat transfer without the use of refractory ceramic

A total of 5 configurations were analyzed, corresponding to 5 positions of the producer gas inlet, as presented in Tab. 6. Figure 8b illustrates the dimension of the variable in the examined design.

The results obtained from the numerical simulations are shown in Figure 11. The set convergence criterion (< 1×10^{-4}) was met shortly before the 18750^{th} iteration, corresponding to a total computational time of approximately 45 minutes. Based on the simulation results it was found that the most favorable impact on heat transfer is achieved by configuration p_5 (highlighted in gold), in which the producer gas inlet is located closest to the boiler water inlet, i.e. at the opposite to the flue gas outlet. In this case, the flue gas has the longest residence time in the combustion chamber and the highest temperature difference between the flue gas and the boiler water. This results in the maximum heat transfer from the flue gas to the boiler water of 13176 W. In contrast, in the least favorable configuration p_1, a larger portion of the gas (approximately 50%) immediately exits the combustion chamber, and consequently decreases radiative heat transfer. As a result, in the total heat transfer from the flue gas to the boiler water, the convective mechanism contributes 10365 W, representing 36.3%. The difference between the most and least favorable configurations is 2.8 kW. Therefore, without refractory ceramic, the effect of extended gas residence time is eliminated, and the most efficient configuration positions the producer gas inlet opposite the combustion chamber gas outlet.

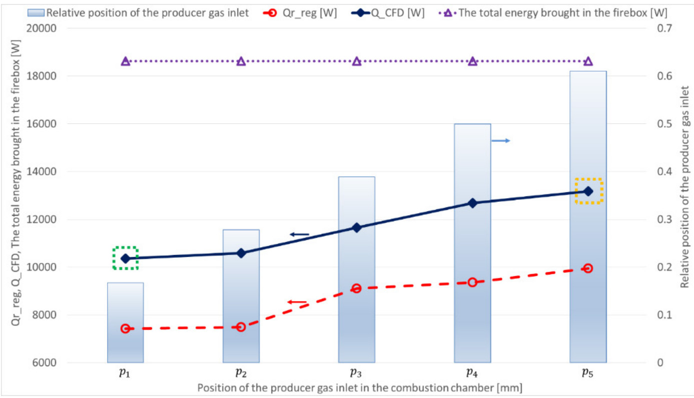

Figure 11. Influence of the producer gas inlet position on heat transfer without the use of refractory ceramic

By applying regression analysis, a mathematical equation describing the heat transferred by radiation (in watts) from the flue gas to the boiler water was obtained and is expressed as follows:

$$Q_{r\_reg} = c_0 + c_1 \cdot p_r + c_2 \cdot \Delta T_{gas} + c_3 \cdot \Delta T_{water} \quad (2)$$

Where c_i are the constants listed in Table 8.

Table 8. Constants used in equation 2

c_0	c_1	c_2	c_3
5288.05	15740.59	45.94	-318.98

Figure 12a presents the results of the numerical simulation for the most favorable configuration p_5, with emphasis on the flue gas temperature field. In this optimal configuration, the producer gas inlet is positioned farthest from the outlet of the combustion chamber to ensure sufficient residence time for heat transfer from the gas to the boiler water. The flue gas temperatures at the outlet of the combustion chamber ranged from 432 to 498 °C. The simulations showed that the water temperature increases, on average, by 10 to 16 °C during heat exchange within the combustion chamber. Figure 12b presents the results of the numerical simulation of the least favorable configuration, p_1.

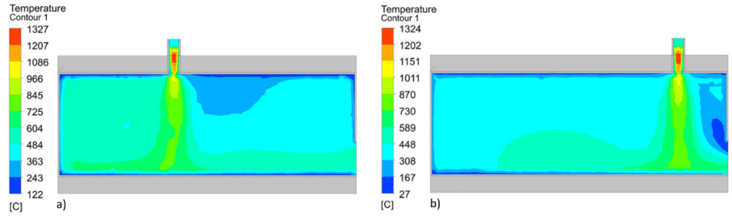

Figure 12. Results of the CFD simulations for the heat transfer in the combustion chamber without refractory ceramics. **a)** the most favorable configuration p_5, **b)** the least favorable configuration p_1

4.3. Influence of the inclination angle of the refractory ceramic on heat transfer

For the producer gas inlet position p_4 (see Tab. 6), a total of 18 configurations were analyzed. These configurations include seven inclination angles of the refractory ceramic relative to the longitudinal axis of the combustion chamber, and three lengths of the refractory ceramic, as presented in Tab. 9. Figure 8c illustrates the variable parameters that define the examined designs.

Table 9. Angles at which the refractory ceramic is positioned relative to the longitudinal axis of the combustion chamber, and the corresponding lengths of the refractory ceramic

Angles at which the refractory ceramic is positioned (θ_i)	Refractory ceramic length (l_i)
θ_1=0 °	l_1=250 mm
θ_2=5 °	l_2=375 mm
θ_3=10 °	l_3=500 mm
θ_4=15 °	
θ_5=22.5 °	
θ_6=30 °	
θ_7=45 °	

The results obtained from the numerical simulations are shown in Figure 13. The set convergence criterion (< 1×10^{-4}) was met shortly before the 14800th iteration, corresponding to a total computational time of approximately 40 minutes. Based on the simulation results, two configurations (θ_1l_1 and θ_2l_1, highlighted in gold) were identified as the most favorable from the perspective of heat transfer. The total heat transferred from the flue gas to the water differs only slightly between the two variants, ranging from 12445 to 12477 W. In wood-log gasification boilers, the producer gas may contain significant amounts of particulates and tar. To promote the separation of particles carried by the producer gas stream leaving the gasification zone, the refractory ceramic is often installed at an angle to the combustion chamber's longitudinal axis. For this reason, configuration θ_2l_1 was selected as the optimal solution, in which the refractory ceramic is inclined at an angle of 5°, with a ceramic length of 250 mm. The least favorable configurations are also shown in Figure 13 (highlighted in green) and are denoted as θ_5l_1 and θ_5l_2. As in the previous case, the total heat transfer values for these variants differ only slightly, ranging from 11148 to 11155 W. Consequently, the difference between the most favorable and the least favorable configurations amounts to 1.33 kW.

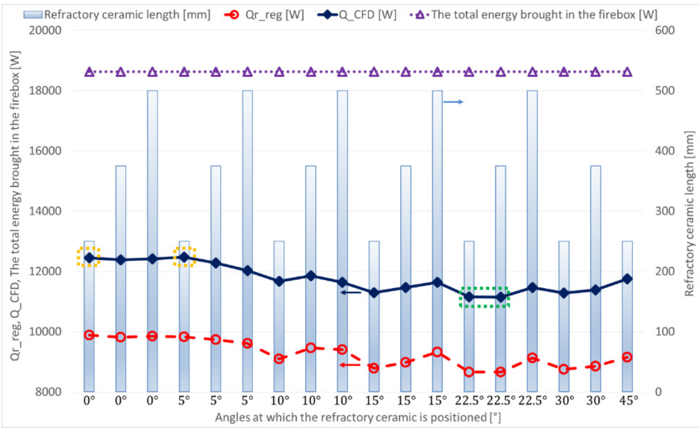

Figure 13. Influence of the inclination angle of the refractory ceramic on heat transfer

By applying regression analysis, a mathematical equation describing the heat transferred by radiation, in watts, from the flue gas to the boiler water was obtained, which is expressed as follows:

$$Q_{r\_reg} = c_0 + c_1 \cdot l + c_2 \cdot \theta + c_3 \cdot \Delta T_{gas} + c_4 \cdot \Delta T_{water} + c_5 \cdot T_{gas_{mean}} + c_6 \cdot T_{water_{mean}} + c_7 \cdot \left(\frac{\Delta T_{gas}}{\Delta T_{water}}\right)^4 + c_8 \cdot \left(\frac{T_{gas_{mean}}}{T_{water_{mean}}}\right)^4 \quad (3)$$

Where c_i are the constants listed in Table 10.

Table 10. Constants used in equation 3

c_0	c_1	c_2	c_3	c_4	c_5	c_6	c_7	c_8
36030.4	1.2385	1.2573	-10.387	429.695	44.855	-197.342	0.457	-144.388

Figure 14a presents the CFD simulation results of the optimal configuration $\theta_2 l_1$, with emphasis on the flue gas temperature field. The 5° inclination primarily promotes radiative heat transfer rather than convection. In this configuration, the slight tilt toward the chamber door is advantageous, as it facilitates the accumulation of particles and ash in close proximity to the refractory ceramic. The flue gas temperatures at the outlet of the combustion chamber ranged from 386 to 445 °C. The simulations showed that the water temperature increased, on average, by 16 to 18 °C during heat exchange within the combustion chamber. Figure 14b presents the CFD simulation results of the least favorable configuration $\theta_5 l_2$. The temperature field is less uniform, with cold zones beneath the refractory ceramic. Additionally, the gas flow deviates to the right through a "short-circuit" path, preventing sufficient residence time for effective heat transfer.

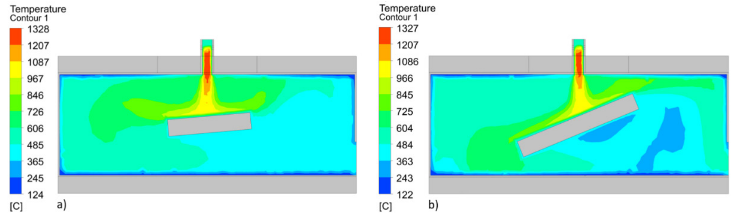

Figure 14. Results of the CFD simulations for the influence of the inclination angle of the refractory ceramic on heat transfer. **a)** the best configuration $\theta_2 l_1$, **b)** the least favorable configuration $\theta_5 l_2$

4.4. Influence of the refractory ceramic distance from the combustion chamber walls and the position of the producer gas inlet on heat transfer

A total of six combinations were analyzed, comprising two distances of the refractory ceramic from the two sides of the combustion chamber and three positions of the producer gas inlet, as presented in Tab. 11. The combinations are denoted in the form $p_i A_i B_i$. Figure 8d illustrates the variable dimensions that define the examined designs. The designs examined divide the flue gas into two streams within the combustion chamber.

Table 11. Distances of the refractory ceramic from the combustion chamber walls and the positions of the fuel gas inlet into the combustion chamber.

Producer gas inlet position (p_i)	Distance of the refractory ceramic from the left wall of the combustion chamber (A_i)	Distance of the refractory ceramic from the right wall of the combustion chamber (B_i)
p_1=300 mm	A_1=150 mm	B_1=50 mm
p_2=450 mm	A_2=200 mm	B_2=100 mm
p_3=600 mm		

The results obtained from the numerical simulations are shown in Figure 15. The set convergence criterion (< 1×10^{-4}) was met shortly before the 12900th iteration, corresponding to a total computational time of approximately 35 minutes. Based on the simulation results, the configuration denoted as $p_1 A_1 B_1$ (highlighted in gold) proved to be the most favorable from the perspective of heat transfer. This configuration achieves the highest heat transfer from the flue gas to the boiler water, amounting to 13176 W. It is characterized by the producer-gas inlet being located on the side opposite the boiler-water inlet, and by smaller distances between the refractory ceramic and the combustion-chamber walls. In addition, Figure 15 shows the least favorable configuration ($p_3 A_2 B_2$, highlighted in green), which results in the lowest heat transfer from the flue gas to the boiler water, amounting to 11670 W. This configuration is characterized by larger distances between the refractory ceramic and the combustion chamber walls, a slightly shorter refractory ceramic length compared to the optimal configuration (a difference of 100 mm), and a producer gas inlet positioned closest to the boiler water inlet. Comparison of the most favorable and least favorable configurations indicates that the difference in heat transfer is 1.33 kW.

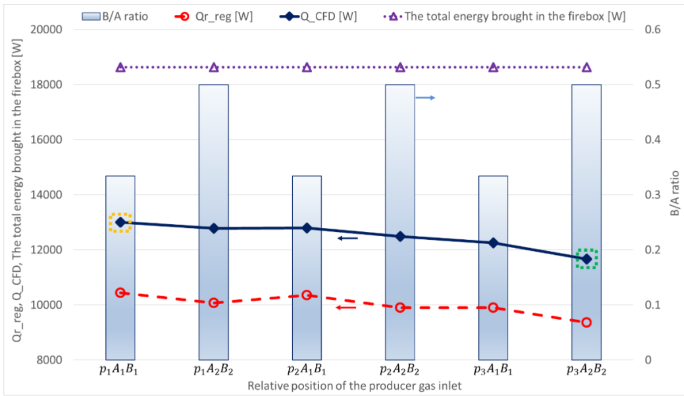

Figure 15. Influence of the refractory ceramic distance from the combustion chamber walls and the position of the producer gas inlet on heat transfer

By applying regression analysis, a mathematical equation describing the heat transferred by radiation, in watts, from the flue gas to the boiler water was obtained, which is expressed as follows:

$$Q_{r\_reg} = c_0 + c_1 \cdot \frac{B}{A} + c_2 \cdot p_r + c_3 \cdot \Delta T_{gas} + c_4 \cdot \Delta T_{water} \quad (4)$$

Where c_i are the constants listed in Table 12.

Table 12. Constants used in equation 4

c_0	c_1	c_2	c_3	c_4
10756.88	-2426.87	-2308.37	2.491	74.31

Figure 16a presents the results of the numerical simulation for the most favorable configuration, $p_1A_1B_1$, with emphasis placed on the flue gas temperature field. The $p_1A_1B_1$ configuration enables prolonged residence time of the flue gas within the combustion chamber and, in combination with the asymmetric spacing of the refractory ceramic (A_1B_1), provides the most efficient heat transfer from the flue gas to the boiler water. The asymmetric clearance of the refractory ceramic in configuration $p_1A_1B_1$ enables a more uniform temperature distribution. The flue gas temperatures at the outlet of the combustion chamber ranged from 382 to 450 °C. The simulations showed that the water temperature increased, on average, by 15 to 18 °C during heat exchange in the combustion chamber. Figure 16b presents the results of the numerical simulation for the most unfavorable configuration, $p_3A_2B_2$. The temperature field is less favorable because a cold zone forms beneath the refractory ceramic. This issue arises because the left-directed flow achieves efficient heat transfer, whereas the right-directed flow follows a "short-circuit" path and does not remain in the chamber long enough to achieve effective heat transfer.

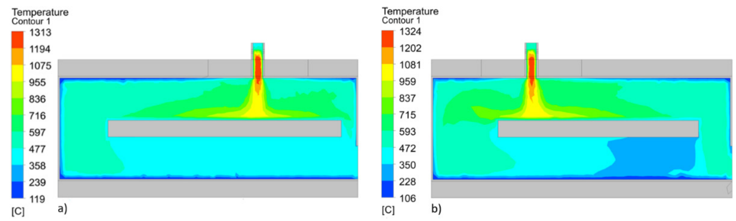

Figure 16. Results of the CFD simulations on the influence of the refractory ceramic's distance from the combustion chamber walls and the position of the producer gas inlet on heat transfer. **a)** the most favorable configuration $p_1A_1B_1$, **b)** the least favorable configuration $p_3A_2B_2$

4.5. Influence of a box-shaped refractory ceramic on heat transfer

For the producer gas inlet position p_1 (see Table 6), a total of 24 configurations were analyzed. Two different refractory ceramic thicknesses, two different heights, two different widths, and three different lengths of refractory ceramic were examined, as presented in Table 13. The configurations are denoted in the form $t_ih_iw_il_i$. Figure 8e illustrates the varying dimensions of the examined design.

Table 13. Different thicknesses, heights, widths, and lengths of the refractory ceramic used in the numerical simulations

Refractory ceramic thickness (t_i)	Refractory ceramic height (h_i)	Refractory ceramic width (w_i)	Refractory ceramic length (l_i)
t_1=25 mm	h_1=150 mm	w_1=180 mm	l_1=300 mm
	h_2=200 mm	w_2=230 mm	l_2=450 mm
			l_3=600 mm
t_2=50 mm	h_1=200 mm	w_1=230 mm	l_1=300 mm
	h_2=250 mm	w_2=280 mm	l_2=450 mm
			l_3=600 mm

The results obtained from the numerical simulations are shown in Figure 17. The set convergence criterion ($< 1\times10^{-4}$) was met shortly before the 18100th iteration, corresponding to a total computational time of approximately 45 minutes. Based on the simulation results, it can be concluded that the most favorable impact on heat transfer is achieved by the configuration denoted as $t_1h_2w_2l_3$ (highlighted in gold). This configuration yields the highest heat transfer rate from the flue gas to the boiler water, amounting to 13337 W. It is characterized by a smaller refractory thickness, greater height and width, and the maximum refractory length considered. Furthermore, Figure 17 also presents the least favorable configuration ($t_1h_1w_1l_2$, highlighted in green), which results in the lowest heat transfer rate from the flue gas to the boiler water, equal to 11864 W. This configuration is characterized by reduced thickness, height, and width, and a refractory length approximately equal to one-half of the combustion chamber length. Comparing the most and least favorable configurations shows that the difference in total heat transfer rate is 1.47 kW.

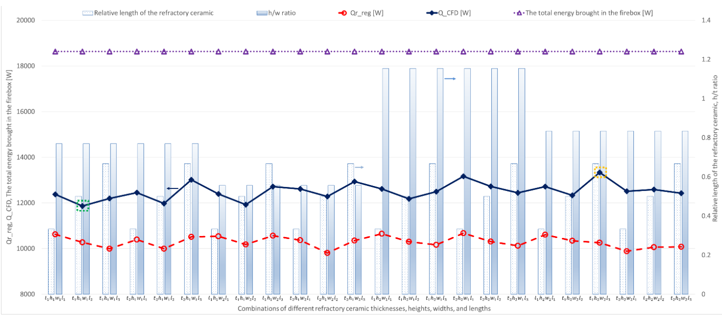

Figure 17. Influence of the geometry of the box-shaped refractory ceramic on heat transfer

By applying regression analysis, a mathematical equation describing the heat transferred by radiation, in watts, from the flue gas to the boiler water was obtained, which is expressed as follows:

$$Q_{r\_reg} = c_0 + c_1 \cdot l_r + c_2 \cdot \frac{h}{t} + c_3 \cdot \Delta T_{gas} + c_4 \cdot \Delta T_{water} + c_5 \cdot \left(\frac{\Delta T_{gas}}{\Delta T_{water}}\right)^2 + c_6 \cdot (\Delta T_{gas} - \Delta T_{water})^2 + c_7 \cdot \left(\frac{T_{gas_{mean}}}{T_{water_{mean}}}\right)^2 + c_8 \cdot (T_{gas_{mean}} - T_{water_{mean}})^2 + c_9 \cdot \left(\frac{\Delta T_{gas}}{\Delta T_{water}}\right)^3 + c_{10} \cdot \left(\frac{T_{gas_{mean}}}{T_{water_{mean}}}\right)^3 + c_{11} \cdot (T_{gas_{mean}} - T_{water_{mean}})^3 + c_{12} \cdot \left(\frac{\Delta T_{gas}}{\Delta T_{water}}\right)^4 + c_{13} \cdot \left(\frac{T_{gas_{mean}}}{T_{water_{mean}}}\right)^4 \quad (5)$$

Where c_i are the constants listed in Tab. 14, and the h/t represents the height-to-width ratio of the refractory ceramic.

Table 14. Constants used in equation 5

c_0	c_1	c_2	c_3	c_4	c_5	c_6
-1433898	-800.687	239.075	8.065	353.769	12.1798	-0.094
c_7	c_8	c_9	c_{10}	c_{11}	c_{12}	c_{13}
1481990	-12.183	3.104	-625992.6	0.02399	-0.2084	71577.172

Figure 18a presents the results of the numerical simulation of the optimal configuration $t_1h_2w_2l_3$, with emphasis placed on the flue gas temperature field. Owing to the greater length of the refractory ceramic, configuration $t_1h_2w_2l_3$ enables prolonged residence of the flue gas within the combustion chamber and, in combination with the increased height and width of the refractory ceramic, achieves the most efficient heat transfer from the flue gas to the boiler water. The dominant contribution to heat transfer arises from radiation emitted by the ceramic and from the narrow gap between the box-shaped ceramic and the combustion-chamber walls; the gap increases gas velocity and consequently enhances convective heat transfer. The primary function of the refractory ceramic is to increase the gas velocity in the region where the coldest flue gas exits the chamber, thereby promoting more effective heat transfer. Based on the simulation results, configuration $t_2h_2w_2l_3$ (with twice the refractory ceramic thickness) achieves a slightly lower heat transfer from the flue gas to the boiler water, amounting to 12427 W, compared to the optimal configuration $t_1h_2w_2l_3$. The flue gas temperatures at the outlet of the combustion chamber ranged from 301 to 503 °C. The simulations showed that the water temperature increased on average by 15–17 °C during heat exchange in the combustion chamber. Figure 18b presents the results of the numerical simulation of the least favorable configuration, $t_1h_1w_1l_2$. The smaller dimensions of the box-shaped refractory ceramic result in a shorter residence time of the flue gas in the combustion chamber, consequently reducing heat transfer from the flue gas to the boiler water.

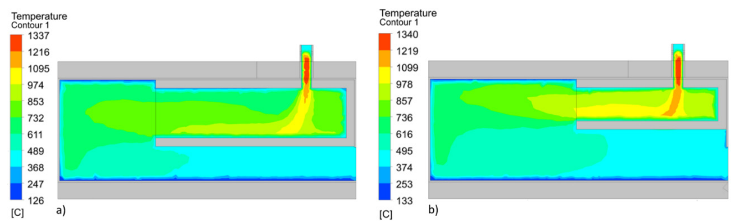

Figure 18. Results of the CFD simulations for the influence of the geometry of the box-shaped refractory ceramic on heat transfer. **a)** the most favorable configuration $t_1h_2w_2l_3$, **b)** the least favorable configuration $t_1h_1w_1l_2$

4.6. Influence of the producer gas composition and combustion air preheating temperature on heat transfer

A total of 18 combinations were analyzed, considering six producer gas compositions and three temperatures of preheated combustion air. The compositions and temperatures of the producer gases were taken from Tab. 5, while the preheated air temperatures were assumed to be T_1=150 °C, T_2=300 °C and T_3=450 °C. The combinations are denoted in the form gc_iT_i, where gc_i represents the producer gas composition, and T_i represents combustion air temperatures. Figure 10a illustrates the geometry used in the examinations.

The results obtained from the numerical simulations are shown in Figure 19. The set convergence criterion ($< 1\times10^{-4}$) was met between 10700 and 15400 iterations, corresponding to a total computational time of approximately 25 to 35 minutes.

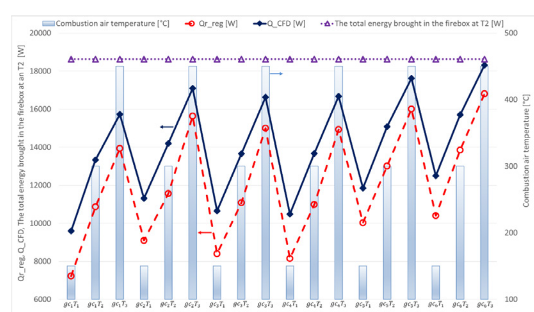

Figure 19. Influence of the producer gas composition and combustion air preheating temperature on heat transfer in the design illustrated in Figure 10 a

Simulation results indicate that air preheating positively affects heat transfer in the combustion chamber. Increasing the combustion air temperature from 150 to 300 °C increases heat transfer by an average of 22.5%. A further increase from 300 to 450 °C adds another 16.1%. The configurations gc_5T_2 and gc_6T_2, corresponding to the gas compositions at CBP-SRC and CBP-PA listed in Tab. 5, achieve a significantly higher heat transfer from the flue gas to the boiler water at a preheated air temperature of 300 °C compared to the other configurations with gas compositions given in columns 1–4 of Tab. 5. This behavior can be attributed to the substantially higher fractions of carbon monoxide and hydrogen in the fuel gas. Excluding the producer gas compositions corresponding to the optimal gasification points, the most favorable configurations for each preheated air temperature are those with the gas composition listed in column 2 of Tab. 5, denoted as gc_2T_1, gc_2T_2, and gc_2T_3. The total heat transfer from the flue gas to the boiler water for these configurations amounts to 11308 W, 14200 W, and 17087 W, respectively. This can be explained by the highest producer-gas temperature (618 °C; Tab. 5) compared with the values in columns 1, 3, and 4, and by a slightly higher tar content. Comparison of the most and least favorable configurations at different preheated-air temperatures revealed that the difference in total heat transfer ranges from 0.9 to 1.7 kW. The least favorable configurations are identified as gc_1T_1, gc_1T_2, and gc_1T_3, which correspond to the gas composition presented in column 1 of Tab. 5. From the heat transfer perspective, these configurations perform the worst due to the relatively lower fuel gas temperature (497 °C, Tab. 5) and significantly lower contents of combustibles (CO, CH_4, H_2) in the producer gas.

By applying regression analysis, a mathematical equation describing the heat transferred by radiation, in watts, from the flue gas to the boiler water was obtained, which is expressed as follows:

$$Q_{r\_reg} = c_0 + c_1 \cdot r_{CO} + c_2 \cdot r_{CH_4} + c_3 \cdot r_{H_2} + c_4 \cdot r_{C_7H_{16}} + c_5 \cdot T_{air} + c_6 \cdot \sqrt{\frac{\Delta T_{gas}}{\Delta T_{water}}} + c_7 \cdot \left(\frac{\Delta T_{gas}}{\Delta T_{water}}\right)^3 + c_8 \cdot \left(\frac{T_{gas_{mean}}}{T_{water_{mean}}}\right)^3 + c_9 \cdot \left(\frac{T_{gas_{mean}}}{T_{water_{mean}}}\right)^4 \quad (6)$$

Where c_i are the constants listed in Tab. 15, r_i represent the volumetric fractions of the combustible components in the producer gas, and T_{air} denotes the temperature of the preheated combustion air.

Table 15. Constants used in equation 6

c_0	c_1	c_2	c_3	c_4
2807.435	-1429.229	-11627.498	-1036.993	-37724.378
c_5	c_6	c_7	c_8	c_9
5.369	256.673	-0.13297	64.02	91.163

Figure 20a presents the results of the numerical simulation of the most favorable configuration, gc_2T_3, corresponding to a preheated combustion air temperature of 450 °C. This configuration is characterized by a higher flue gas velocity (i.e., enhanced convective effects) at the outlet of the combustion chamber than in the least favorable configuration. Emphasis is placed on the flue-gas temperature field. The analyzed variant achieves the highest heat transfer rate from the flue gas to the boiler water, equal to 17087 W.

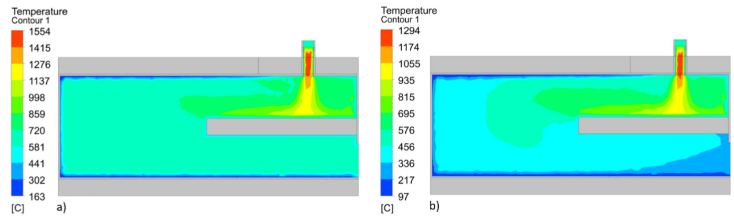

Figure 20. Results of the CFD simulations for the influence of the producer gas composition and combustion air preheating temperature on heat transfer in the design illustrated in Figure 10a. **a)** the most favorable configuration gc_2T_3 for preheated combustion air temperature of 450 °C, **b)** the least favorable configuration gc_1T_1, for preheated combustion air temperature of 150 °C

Ideally, the air should be preheated for both gasification and combustion, while the gasification process should operate as close as possible to its optimal conditions. Furthermore, the producer gas with a higher heating value is desirable because it enables greater heat transfer in the combustion chamber. The flue gas temperatures at the outlet of the combustion chamber ranged from 288 to 770 °C. The simulations showed that the water temperature increased, on average, by 11 to 28 °C during heat exchange in the combustion chamber. Figure 20b presents the results of the numerical simulation for the least favorable configuration, gc_1T_1. This configuration achieves the lowest heat transfer from the flue gas to the boiler water, amounting to 9593 W. It is characterized by a lower producer gas temperature at the inlet of the combustion chamber and the lowest combustion air temperature (150 °C).

4.7. Effect of adding a 50 mm thick refractory at the boiler door to the existing U shaped flow path refractory

Following the approach adopted in Section 4.1, a total of 25 configurations were analyzed, comprising combinations of five refractory ceramic lengths and five producer-gas inlet positions. Compared to the aforementioned section, the only difference is an additional 50-mm-thick refractory ceramic installed on the boiler door. Figure 8f illustrates the examined design.

The results obtained from the numerical simulations are shown in Figure 21. The set convergence criterion ($< 1\times10^{-4}$) was met shortly before the 13000^{th} iteration, corresponding to a total computational time of approximately 35 minutes.

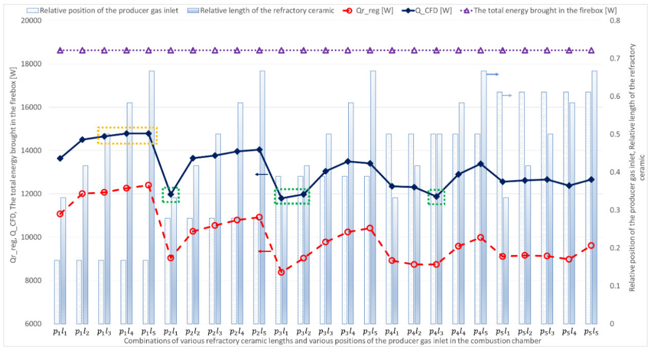

Figure 21. Influence of the addition of the 50 mm thick refractory at the boiler door to the existing U-shaped flow path refractory

Similarly to Section 4.1, the most favorable configurations in this case were those in which the producer gas inlet is positioned closest to the flue gas outlet and the refractory ceramic has a minimum length of approximately half the chamber length (configurations p_1l_3, p_1l_4, and p_1l_5, highlighted in gold). The total heat transferred from the flue gas to the boiler water varies minimally among the three configurations, ranging from 14653 to 14787 W. The least favorable configurations can also be observed in Figure 21 (highlighted in green) and are denoted as p_2l_1, p_3l_1, p_3l_2, and p_4l_3, with total heat transfer values varying only slightly, ranging from 11796 to 11979 W. Consequently, the difference between the most and least favorable configurations amounts to approximately 3 kW.

The radiative heat transfer is calculated using the same eq. (1) as presented in Section 4.1, with different constant values listed in Table 16.

Table 16. Constants used in equation 1

c_0	c_1	c_2	c_3	c_4	c_5	c_6
-393553.71	-486.25	2021.56	-1680.71	32.422	0.1965	352100.35
c_7	c_8	c_9	c_{10}	c_{11}	c_{12}	
2706.91	-17.349	-180367.34	-921.58	1.6521	26082.31	

Similarly to Section 4.1, configuration p_1l_3 was selected as optimal. Comparison of the optimal configurations identified in this section with those reported in Section 4.1 shows that the additional refractory ceramic installed at the boiler door improves heat transfer by approximately 9.9%. Figure 22a presents the results of the numerical simulation for the optimal configuration, with particular emphasis placed on the temperature field of the flue gas. The flue gas temperatures at the outlet of the combustion chamber ranged from 425 to 546 °C. The simulations showed that the water temperature increased on average by 9–20 °C during heat exchange in the combustion chamber.

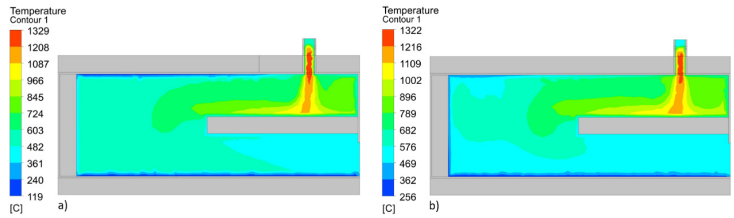

Figure 22. CFD simulation results showing the influence on heat transfer of adding a 50-mm-thick refractory at the boiler door to the existing U-shaped flow path refractory. **a)** the best configuration p_1l_3, **b)** the best configuration p_1l_3 (see. 4.8)

4.8. Effect of adding added refractory elements to the existing U-shaped flow path refractory

The subsection analyzes the case in which the majority of the combustion chamber is coated with refractory elements. Figure 8g illustrates the design. Following the approach adopted in Section 4.1, a total of 25 configurations were analyzed, including five refractory ceramic lengths and five producer gas inlet positions. Compared with the aforementioned section, two differences can be identified: an additional 50 mm-thick refractory ceramic installed at the boiler door and additional refractory installed along the entire length of the combustion chamber.

The results obtained from the numerical simulations are shown in Figure 23. The set convergence criterion ($< 1\times10^{-4}$) was met shortly before the 13000th iteration, corresponding to a total computational time of approximately 35 minutes. Similarly to Section 4.1.1, the most favorable configurations were p_1l_3, p_1l_4, and p_1l_5 (highlighted in gold). The total heat transferred from the flue gas to the boiler water varies minimally across the three configurations, ranging from 16265 to 16539 W. The least favorable configurations were p_2l_1, p_3l_1, p_4l_2, and p_4l_3 (highlighted in green), with total heat transfer values varying only slightly, ranging from 12900 to 13388 W. Consequently, the difference between the most and least favorable configurations amounts to approximately 3.64 kW.

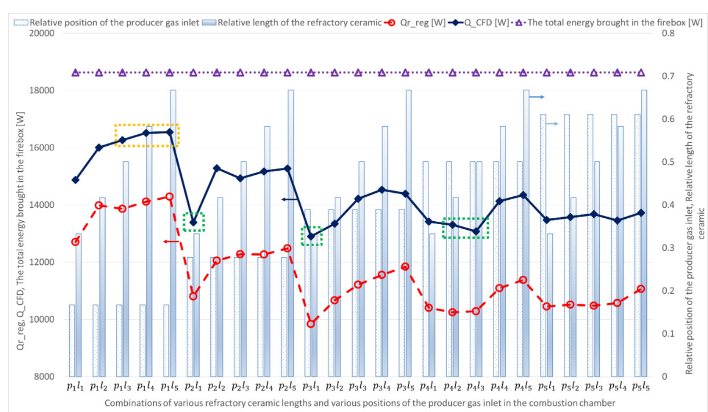

Figure 23. Influence of coating the majority of the combustion chamber with refractories

Figure 22b presents the results of the numerical simulation for the best configuration, with particular emphasis on the temperature field of the flue gas. The flue gas temperatures at the outlet of the combustion chamber ranged from 418 to 545 °C. The simulations showed that the water temperature increased, on average, by 8 to 20 °C during heat exchange within the combustion chamber. Comparison of the optimal configurations identified in this section with those reported in Section 4.1 shows that adding refractory ceramic to the boiler door and to the entire top length of the combustion chamber improves heat transfer by approximately 22%, despite a 17% smaller heat-exchange surface area. While both cases exhibit identical convective heat transfer, the additional ceramic elements in this configuration enhance radiative heat transfer. These elements help equalize temperatures across a larger volume of the combustion chamber and are directly exposed to heat transfer surfaces.

The radiative heat transfer is calculated using the same eq. (1) presented in Section 4.1.1, but with different constant values listed in Tab. 17.

Table 17. Constants used in equation 1

c_0	c_1	c_2	c_3	c_4	c_5	c_6
-928530.81	606.944	467.46	-9063.54	106.175	0.0321	-928530.81
c_7	c_8	c_9	c_{10}	c_{11}	c_{12}	
9078.63	-43.786	-398876.68	-2483.277	4.47	56211.865	

The fit statistics for the eight regression equations are summarized in Table 18. All models exhibit high coefficients of determination (R^2), ranging from 0.947 to 0.999, indicating that they capture a large fraction of the variance in the CFD data. A more comprehensive assessment is provided by the adjusted R^2, which accounts for the number of predictors, and by the error metrics (RMSE and MAPE). Equations 2, 6, and 7 demonstrate excellent performance, with both R^2 and adjusted R^2 being above 0.989 and with relatively low RMSE and MAPE. Equation 3, while exhibiting a slightly lower adjusted R^2 (0.970), achieves the lowest RMSE (76.53 W), making it the most accurate in terms of absolute error. Equation 8 also exhibits high R^2 values (0.987/0.975), but it's RMSE (212.65 W) is the highest among the models, indicating a poorer fit despite good explanatory power. In contrast, Eqs. 4 and 5 exhibit a more pronounced drop from R^2 and adjusted R^2 (from 0.954 to 0.771 and from 0.947 to 0.827, respectively), suggesting that these models may include terms that do not substantially enhance predictive capability. Overall, while all models achieve high R^2, the combined metrics suggest that Eqs. 2, 3, and 7 offer the best balance between accuracy and complexity. Equations 4 and 5 could be further simplified in future work to improve parsimony without significantly compromising accuracy.

Table 18. Fit statistics for the regression equations (Equations 1–8)

Equation	R^2	adjusted R^2	RMSE (W)	MAPE (%)
1	0.981	0.961	196.50	0.94
2	0.998	0.992	102.78	0.37
3	0.984	0.970	76.53	0.49
4	0.954	0.771	189.05	0.71
5	0.947	0.827	105.92	0.45
6	0.999	0.998	168.91	1.92
7	0.994	0.989	127.44	0.61
8	0.987	0.975	212.65	0.96

Equations 1-6 are applicable to all wood-log gasification boilers with boxy combustion chambers operating with approximately 7% of O2 in dry flue gas.

In the presented results, the combustion chamber volume heat release rate corresponds to the literature [42-44]. It is even slightly lower than the value of 250–330 kW/m³ recommended by Wang et al. [46], who experimented with corn straw briquettes and a different combustor design. Additionally, the average convective heat transfer coefficient across all simulations is 7.6 W/m²K, which corresponds to the recommended values [47].

5. Conclusion

The paper analyzes practical issues concerning the design of combustion chambers in wood-log gasification boilers, a topic well known to boiler manufacturers but scarcely addressed in the scientific literature. The main conclusions are:

- Both experimental and CFD results indicate that the optimal shape and placement of ceramic elements and the overall thermal performance of the combustion chamber depend on the design of the gasification chamber. This dependency exists because the producer gas composition, which is determined by the gasification chamber design, plays a crucial role in heat transfer.
- For a given combustion chamber, optimal thermal performance is achieved with the theoretical producer-gas composition corresponding to the carbon-boundary point. This indicates that higher chemical energy content in the gas (resulting from complete gasification), together with elevated gas temperature and the use of preheated combustion air, significantly increases radiative heat flux. This enhanced radiation, in turn, enables a more compact and efficient chamber design.
- A comparison of the results shows that refractory elements that create a U-shaped flue-gas flow path inside the combustion chamber (Figures 9, 10, 17, 18, 20, 21) are the most effective for overall heat transfer. To establish this U-shaped flow path, the element must extend at least half the length of the combustion chamber. This configuration places the producer gas combustion zone above the flue gas outlet (Figures 10, 18, 20) and prolongs the flue gas residence time. The heights of the producer-gas combustion zone and the flue-gas channels on the element should be asymmetric, with the flue-gas channel having the smaller flow cross-section (Figures 10, 18). In this case, both radiative heat transfer from the refractory element and convective heat transfer from the cooler flue gas are

increased.
- The total heat transfer values for the U-shaped flow path elements, the elements that divide the flue gas stream (Figures 13–16), and the case without ceramics are similar: 13498 W, 13176 W, and 13176 W, respectively. Nevertheless, the U-shaped flow path is slightly advantageous not only for total heat transfer but also for particulate and ash removal, owing to the U-turn in front of the chamber opening.
- If ceramic elements are omitted, the producer gas inlet should be placed on the side opposite the flue gas outlet. To protect the metal surface of the bottom wall directly opposite the gas inlet, a small ceramic piece should be installed, preferably inclined by 5° away from the flue gas outlet. This slight inclination promotes the agglomeration of fly ash and particulates near the chamber door and increases the flue gas residence time.
- Additional refractory elements installed at the boiler door and separating the gasification and combustion chambers further enhance heat transfer, indicating that new refractory elements should be positioned within the field of view of the heat transfer surfaces. The conclusion is supported by the observation that, in the analyzed case, the additional ceramic elements in the combustion chamber reduce the heat exchange surface area by 17% while simultaneously improving heat transfer by 22%.

Future work to extend the scientific impact of this study includes the mathematical description of the use of ceramic elements in alternative combustion chamber designs and in vortex combustion. Such work should specifically address the effects of these elements on heat transfer, emissions, and combustion completeness.

Authorship contributions

Conceptualization, Đ.A.N.; methodology, Đ.A.N., R.M.K., and M.V.N.; software, Đ.A.N., and M.V.N.; validation, D.M.T., M.O.O., R.M.K., Đ.A.N., and M.V.N.; formal analysis Đ.A.N., R.M.K., and M.V.N.; investigation, Đ.A.N., R.M.K., and M.V.N.; resources, D.M.T., and M.O.O.; data curation, D.M.T., and M.O.O.; writing—original draft preparation, Đ.A.N., and R.M.K.; writing—review and editing, M.V.N., D.M.T., and M.O.O.; visualization, Đ.A.N.; supervision, R.M.K., and M.V.N. All authors have read and agreed to the published version of the manuscript.

Conflict of interest

The authors declared no potential conflicts of interest with respect to the research, authorship, and/or publication of this article.

Data availability statement

Data will be made available on request.

Declaration of generative AI and AI-assisted technologies in the writing process

During the preparation of this manuscript, the authors used ChatGPT (OpenAI) solely to improve the grammar, language, and readability of the text. The authors reviewed and edited the output as necessary and take full responsibility for the content of the manuscript.

Acknowledgement

This research was supported by the Science Fund of the Republic of Serbia (Grant No. 5959, Active Condensation Hybrid Systems in Biomass Combustion, AC-BC).

References

[1] “IEA - International Energy Agency.”
[2] “Distribution of bioenergy consumption worldwide in 2022, by biomass type.” Accessed: January 12, 2026. https://www.statista.com/statistics/1496484/share-of-global-consumption-of-bioenergy-by-biomass-type/
[3] “Wood Log Gasification Boilers 2026 to Grow at XX CAGR with 601 million Market Size: Analysis and Forecasts 2033.” Accessed: January 12, 2026. https://www.archivemarketresearch.com/reports/wood-log-gasification-boilers-202915?utm_source=chatgpt.com
[4] A. Bukar, M. Ben Oumarou, B. M. Tela, and A. M. Eljummah, “Assessment of Biomass Gasification: A Review of Basic Design Considerations,” American Journal of Energy Research, vol. 7, no. 1, pp. 1–14, 2019. doi: 10.12691/ajer-7-1-1.
[5] Karamarković, D. Todorović, Đ. Novčić, M. Obradović, and M. Nikolić, “Eksperimentalna ispitivanja gasifikacione komore kotla na drva,” in Zbornik Međunarodnog kongresa o procesnoj industriji - Procesing, pp. 63–72, 2023. https://izdanja.smeits.rs/index.php/ptk/article/view/6869/7052
[6] Sengupta, “Refractories for the Chemical Industries.” 2020. https://doi.org/10.1007/978-3-030-61240-5
[7] C. Gupta, “Fuels, Furnaces and Refractories.” PHI Learning, 2017.
[8] Terzić, “Uticaj mikrostrukture na svojstva vatrostalnih betona,” Univerzitet u Beogradu, 2009. https://nardus.mpn.gov.rs/bitstream/id/17779/Disertacija.pdf
[9] Martinović, “Ispitivanje uticaja temperature sinterovanja na termostabilnost niskocementnih visokoaluminatnih vatrostalnih betona,” Univerzitet u Beogradu, 2011. https://core.ac.uk/download/296573126.pdf
[10] “Fire Brick and Refractory Brick.” Accessed: Jul. 12, 2025. https://brickwoodovens.com/pages/fire-brick
[11] Harbison-Walker, “Harbison-Walker Handbook of Refractory Practice,” 2005.

[12] Buchmayr, J. Gruber, M. Hargassner, and C. Hochenauer, “Experimental investigation of the primary combustion zone during staged combustion of wood-chips in a commercial small-scale boiler,” Biomass and Bioenergy, vol. 81, pp. 356–363, 2015. https://doi.org/10.1016/j.biombioe.2015.07.016

[13] Caposciutti, H. Almuina-Villar, A. Dieguez-Alonso, T. Gruber, J. Kelz, U. Desideri, C. Hochenauer, R. Scharler, and A. Anca-Couce, “Experimental investigation on biomass shrinking and swelling behaviour: Particles pyrolysis and wood logs combustion,” Biomass and Bioenergy, vol. 123, pp. 1–13, 2019. https://doi.org/10.1016/j.biombioe.2019.01.044

[14] Kirch, P. R. Medwell, C. H. Birzer, and P. J. van Eyk, “Feedstock Dependence of Emissions from a Reverse-Downdraft Gasifier Cookstove,” Energy for Sustainable Development, vol. 56, pp. 42–50, 2020. https://doi.org/10.1016/j.esd.2020.02.008

[15] Kirch, P. R. Medwell, C. H. Birzer, and P. J. Van Eyk, “Influences of Fuel Bed Depth and Air Supply on Small-Scale Batch-Fed Reverse Downdraft Biomass Conversion,” Energy and Fuels, vol. 32, no. 8, pp. 8507–8518, 2018. https://doi.org/10.1021/acs.energyfuels.8b01699

[16] Chanphavong, K. A. Al-Attab, and Z. A. Zainal, “Flameless Combustion Characteristics of Producer Gas Premixed Charge in a Cyclone Combustor,” Flow, Turbulence and Combustion, vol. 103, no. 3, pp. 731–750, 2019. https://doi.org/10.1007/s10494-019-00043-x

[17] Drosatos, A. Nesiadis, N. Nikolopoulos, N. Margaritis, P. Grammelis, and E. Kakaras, “CFD Simulation of Domestic Gasification Boiler,” Journal of Energy Engineering, vol. 143, no. 2, pp. 1–19, 2017. https://doi.org/10.1061/(ASCE)EY.1943-7897.0000406

[18] Trojanowski, T. Butcher, and V. Fthenakis, “The Impact of Fuel Type and Burn Phase on Combustion-Related Emissions and Efficiency of Woodchip-Fired Boilers,” Energy & Fuels, vol. 38, no. 21, pp. 21308-21321, 2024. https://doi.org/10.1021/acs.energyfuels.4c00833

[19] Hopan, M. Chmelar, J. Kremer, M. Dej, M. Vojtisek-Lom, E.D. Vicente, J. Rysavy, K. Krpec, L. Kubonova, A. Molcanov, M. Schwabl, and J. Horak, “In-situ investigation of real-world emissions from 111 measurements on solid fuel household boilers,” Science of The Total Environment, vol. 981, 179564, 2025. https://doi.org/10.1016/j.scitotenv.2025.179564

[20] Kateria and K. Sornek, “Biomass for Residential Heating: A Review of Technologies, Applications, and Sustainability Aspects,” Energies, vol. 18, no. 22: 5875, 2025. https://doi.org/10.3390/en18225875

[21] Hasler and T. Nussbaumer, “Sampling and analysis of particles and tars from biomass gasifiers,” Biomass and Bioenergy, vol. 18, no. 1, pp. 61–66, 2000. https://doi.org/10.1016/S0961-9534(99)00071-9

[22] Karamarkovic and V. Karamarkovic, “Energy and exergy analysis of biomass gasification at different temperatures,” Energy, vol. 35, no. 2, pp. 537–549, 2010. https://doi.org/10.1016/j.energy.2009.10.022

[23] M. Karamarković, V. M. Karamarković, A. M. Jovović, M. R. Marašević, and A. D. Lazarević, “Biomass gasification with preheated air: Energy and exergy analysis,” Thermal Science, vol. 16, no. 2, pp. 535–550, 2012. https://doi.org/10.2298/TSCI110708011K

[24] Desrosiers, “Thermodynamics of gas-char reactions,” in A Survey of Biomass Gasification, Solar Energy Research Institute (SERI), Golden, CO, 1979.

[25] Jalili, K. Kazerani, B. Jalili, and D. D. Ganji, “Investigation of thermal analysis and pressure drop in non-continuous helical baffle with different helix angles and hybrid nano-particles,” Case Studies in Thermal Engineering, vol. 36, 102209, 2022. https://doi.org/10.1016/j.csite.2022.102209

[26] Rajak, P. Nashine, P. K. Chaurasiya, and T. Nath Verma, “A numerical investigation of the species transport approach for modeling of gaseous combustion,” Journal of Thermal Engineering, vol. 7, no. Supp 14, pp. 2054–2067, 2021. https://doi.org/10.18186/thermal.1051312

[27] Abay, U. Colak, and L. Yuksek, “Computational fluid dynamics analysis of flow and combustion of a diesel engine,” Journal of Thermal Engineering, vol. 4, no. 2, pp. 1878-1895, 2018. https://doi.org/10.18186/journal-of-thermal-engineering.388333

[28] Jalili, N. Aghaee, P. Jalili, and D. Domiri, “Novel usage of the curved rectangular fin on the heat transfer of a double-pipe heat exchanger with a nanofluid,” Case Studies in Thermal Engineering, vol. 35, 102086, 2022. https://doi.org/10.1016/j.csite.2022.102086

[29] K. Patel and A. D. Parekh, “Thermal design and CFD simulation of an internal heat exchanger with R1234yf as an alternate refrigerant to R134a,” Journal of Thermal Engineering, vol. 11, no. 5, pp. 1339–1354, 2025. https://doi.org/10.14744/thermal.0000998

[30] G. Nugraha, H. Saptoadi, M. Hidayat, B. Andersson, and R. Andersson, “Particulate matter reduction in residual biomass combustion,” Energies, vol. 14, no. 11, 2021. https://doi.org/10.3390/en14113341

[31] “ANSYS FLUENT 12.0 Theory Guide - 4.12.2 Standard Wall Functions.” Accessed: July 16, 2025. https://www.afs.enea.it/project/neptunius/docs/fluent/html/th/node99.htm

[32] “Ansys Mesh Metrics Explained.” Accessed: July 16, 2025. https://www.mechead.com/mesh-quality-checking-ansys-workbench/

[33] Osterode A., “D6 Properties of Solids and Solid Materials,” VDI Heat Atlas, Springer, pp. 581–590, 2010. https://doi.org/10.1007/978-3-540-77877-6_26

[34] “Refractory Materials with Good Wear Resistance for Boilers.” Accessed: June 11, 2026. https://refractoriesmaterials.com/refractory-materials-with-good-wear-resistance-for-boilers/

[35] “Wear-Resistant Refractory Materials for CFB Boilers.” Accessed: June 11, 2026. https://xintairefractory.com/wear-resistant-refractory-materials-for-cfb-boilers/

[36] LI, E. Vainio, L. Hupa, M. Hupa, and E. Zabetta, “High-temperature corrosion of refractory materials in biomass and waste combustion: method development and tests with alumina refractory exposed to a K2CO3–KCl mixture,” Energy and Fuels, vol. 31, no. 9, pp. 10046–10054, 2017. https://doi.org/10.1021/acs.energyfuels.7b01123
[37] Han, Z. Wang, B. Liu, Y. Huang, and S. Su, “In-situ improved corrosion resistance of corundum-mullite refractory for the incineration of hazardous spent high-salt organic liquor by Cr2O3: Interfacial anti-erosion mechanism,” Ceramics International, vol. 48, no. 9, pp. 12395–12407, 2022. https://doi.org/10.1016/j.ceramint.2022.01.104
[38] John R. Howell, M. Pinar Mengüc, Kyle Daun, and Robert Siegel, “Thermal Radiation Heat Transfer,” 7th Edition, 2020. https://doi.org/10.1201/9780429327308
[39] Don W. Green and Robert H. Perry, “Perry’s Chemical Engineers’ Handbook,” 8th Edition, 2008.
[40] “VDI Heat Atlas,” Springer, 2010. https://doi.org/10.1007/978-3-540-77877-6_26
[41] A. Novčić, M. V. Nikolić, D. M. Todorović, R. M. Karamarković, and M. O. Obradović, “EXPERIMENTAL AND CFD ANALYSIS OF WIRE COIL TURBULATORS IN BIOMASS BOILERS,” Thermal Science, vol. 27, no. 1 Part A, pp. 71–87, 2023. https://doi.org/10.2298/TSCI2301071N
[42] “Wood gasification boiler BLAZE GREEN.” Accessed: August 05, 2025. https://www.blazeharmony.com/en/www/wood-boilers/gasification-boiler-blaze-green
[43] “Wood and coal gasification boiler ORLAN SUPER.” Accessed: August 05, 2025. https://kotly.com/gb/1766-wood-and-coal-gasification-boiler-orlan-super.html
[44] “S3 Turbo wood boiler.” Accessed: August 05, 2025. https://www.froeling.com/en-gb/products/firewood-boiler/s3-turbo/
[45] “Microsoft Excel.” Accessed: August 06, 2025. https://www.microsoft.com/en-us/microsoft-365/excel
[46] Wang, L. Liu, Y. Yuan, H. Yang, Y. Zhou, and R. Duan, “Design and key heating power parameters of a newly-developed household biomass briquette heating boiler,” Renewable Energy, vol. 147, part 1, pp. 1371–1379, 2020. https://doi.org/10.1016/j.renene.2019.09.081
[47] Stephan, “B1 Fundamentals of Heat Transfer,” in VDI Heat Atlas, pp. 15–30, 2010. https://doi.org/10.1007/978-3-540-77877-6_115

Appendices

Appendix A. CFD model

Figure A1. Mesh of 3D model

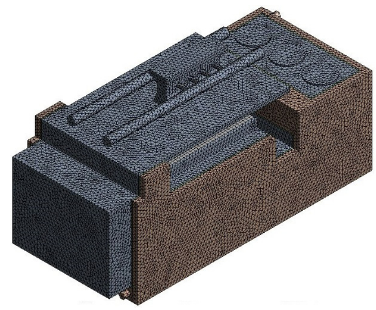

Appendix B. Turbulence model

Table B1. Comparison of turbulence models

standard k-ε	realizable k-ε	RNG k-ε	k–ω SST
Q=13.33 kW	Q=12.68 kW	Q=13.13 kW	Q=14.08 kW
Qr=11.07 kW	Qr=11.2 kW	Qr=12.01 kW	Qr=10.67 kW
Tgas_outlet=468.6 °C	Tgas_outlet=424.5 °C	Tgas_outlet=449.7 °C	Tgas_outlet=486.1 °C
Twater_outlet=72.3 °C	Twater_outlet=74.4 °C	Twater_outlet=75.9 °C	Twater_outlet=73.3 °C

Appendix C. Mesh independence

A mesh refinement study was conducted using four grids, and the results for total heat transfer, flue gas outlet temperature, and representative wall heat flux are summarized in Table C1. It can be observed that the variation between the medium (M2) and fine mesh (M4) is below 3% for all monitored quantities, indicating mesh-independent results. Therefore, the medium mesh was adopted for further simulations as a compromise between accuracy and computational cost.

Table C1. Mesh refinement study

Mesh	Mesh size (cells)	Q [kW]	Tgas_outlet [°C]	q [W/m2]
M1	44680	13.6	515.8	13592
M2	172862	13.33	468.6	13331
M3	951195	13.25	464.22	13248
M4	1469751	13.28	457.6	13277

Since the selected representative surface area is approximately 1 m^2, the reported wall heat flux values closely follow the total heat transfer results. Therefore, both quantities exhibit similar convergence behavior, as expected.

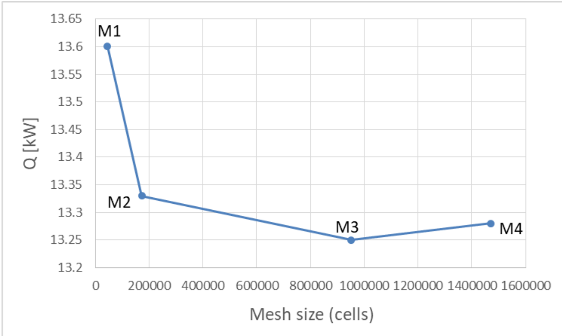

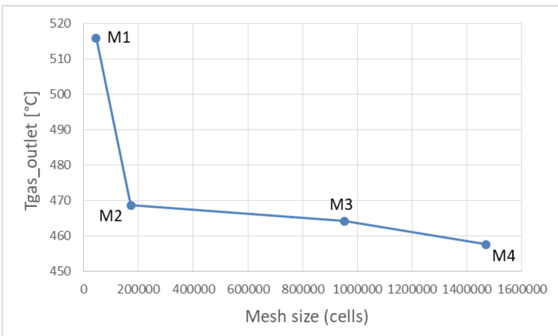

Appendix D. A sensitivity analysis of the angular discretization of the Discrete Ordinates (DO)

A sensitivity analysis of the angular discretization of the Discrete Ordinates (DO) radiation model was performed. Simulations were carried out using 2×2, 4×4, and 6×6 angular divisions. The results showed that the variation in maximum temperature, average temperature, and radiative heat flux between the 4x4 and 6x6 discretizations was below 1%, confirming angular discretization independence. Therefore, a 4×4 angular discretization was used in all simulations to ensure accurate prediction of radiative heat transfer.

DO angular discretization (θ x ϕ)	Tgas_max [°C]	Tgas_mean [°C]	Qr [kW]
2 x 2	1457.77	611.85	11.07
4 x 4	1457.76	611.84	11.05
6 x 6	1457.74	611.84	11.04